

Fall 2002

Modeling of Acoustic Emission Failure Mechanism Data from a Unidirectional Fiberglass/Epoxy Tensile Test Specimen

Daniel R. Lenzioszek
Embry-Riddle Aeronautical University - Daytona Beach

Follow this and additional works at: <https://commons.erau.edu/db-theses>



Part of the [Aerospace Engineering Commons](#)

Scholarly Commons Citation

Lenzioszek, Daniel R., "Modeling of Acoustic Emission Failure Mechanism Data from a Unidirectional Fiberglass/Epoxy Tensile Test Specimen" (2002). *Theses - Daytona Beach*. 119.
<https://commons.erau.edu/db-theses/119>

This thesis is brought to you for free and open access by Embry-Riddle Aeronautical University – Daytona Beach at ERAU Scholarly Commons. It has been accepted for inclusion in the Theses - Daytona Beach collection by an authorized administrator of ERAU Scholarly Commons. For more information, please contact commons@erau.edu.

**MODELING OF ACOUSTIC EMISSION FAILURE MECHANISM DATA FROM
A UNIDIRECTIONAL FIBERGLASS/EPOXY TENSILE TEST SPECIMEN**

by

Daniel R. Lenzioszek

A Thesis Submitted to the Graduate Studies Office
in Partial Fulfillment of the Requirements for the Degree of
Master of Science in Aerospace Engineering

Embry-Riddle Aeronautical University
Daytona Beach, Florida
Fall 2002

UMI Number: EP31895

INFORMATION TO USERS

The quality of this reproduction is dependent upon the quality of the copy submitted. Broken or indistinct print, colored or poor quality illustrations and photographs, print bleed-through, substandard margins, and improper alignment can adversely affect reproduction.

In the unlikely event that the author did not send a complete manuscript and there are missing pages, these will be noted. Also, if unauthorized copyright material had to be removed, a note will indicate the deletion.

UMI[®]

UMI Microform EP31895
Copyright 2011 by ProQuest LLC
All rights reserved. This microform edition is protected against
unauthorized copying under Title 17, United States Code.

ProQuest LLC
789 East Eisenhower Parkway
P.O. Box 1346
Ann Arbor, MI 48106-1346

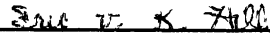
**MODELING OF ACOUSTIC EMISSION FAILURE MECHANISM DATA FROM
A UNIDIRECTIONAL FIBERGLASS/EPOXY TENSILE TEST SPECIMEN**

by

Daniel R. Lenzioszek

This thesis was prepared under the direction of the candidate's thesis committee chairman, Dr. Eric v. K. Hill, Department of Aerospace Engineering, and has been approved by the members of his thesis committee. It was submitted to the Department of Aerospace Engineering and was accepted in partial fulfillment of the requirements for the degree of Master of Science in Aerospace Engineering.

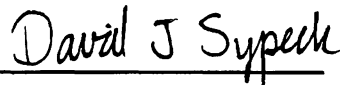
THESIS COMMITTEE



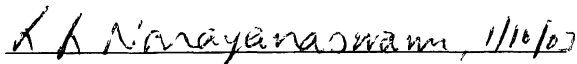
Dr. Eric v. K. Hill
Chairman




Dr. Yi Zhao
Member




Dr. David J. Sypek
Member



Graduate Program Coordinator, MSAE



Department Chair, Aerospace Engineering



Date

ACKNOWLEDGEMENTS

Most importantly I would like to thank my parents. Without their constant encouragement and support, I would have never made it as far as I have. I would like to thank Dr. Eric Hill for providing me the opportunity to remain at Embry-Riddle to do my graduate work. Without his encouragement to stay, and providing me with the opportunity to teach one of the laboratory classes, I would not have been able to perform this work. I would also like to thank Dr. Yi Zhao and Dr. David Sypeck for agreeing to be on my thesis committee with such short time constraints.

I also need to thank several students who have provided help along the way: Anthony Anderson, Travis Robinson, Faisal Samkari, Helene de Causans, Federico Martinez, and Raphaël Cioffi. Without their help in plotting the curves, I might have never made it through all of the different types of analyses. I would also like to thank Robert Demeski for his help in understanding the original data set.

ABSTRACT

Author: Daniel R. Lendzioszek
Title: Modeling of Acoustic Emission Failure Mechanism Data from
a Unidirectional Fiberglass/Epoxy Tensile Test Specimen
Institution: Embry-Riddle Aeronautical University, Daytona Beach
Degree: Master of Science in Aerospace Engineering
Year: 2002

The purpose of this work was to model the acoustic emission (AE) flaw growth data that resulted from the tensile test of a unidirectional fiberglass/epoxy specimen. The data collected and stored during the test were the six standard AE quantification parameters for each event. A classification neural network was used to sort the data into five failure mechanism clusters. The resulting frequency histograms of the sorted data were then mathematically modeled herein using the three types of Johnson distributions: bounded, lognormal, and unbounded. These provided a reasonably good fit for all six AE parameter distributions for each of the five failure mechanisms.

TABLE OF CONTENTS

	Page
ABSTRACT.....	iii
TABLE OF CONTENTS.....	iv
LIST OF TABLES.....	vi
LIST OF FIGURES	vii
1.0 INTRODUCTION	1
1.1 Overview.....	1
1.2 Previous Research.....	1
1.3 Current Approach.....	3
2.0 THEORY	4
2.1 Acoustic Emission	4
2.2 AE Signal Parameters	4
2.3 Initial Settings	5
2.4 Composite Failure Mechanisms.....	6
2.5 Classification of Failure Mechanisms.....	6
2.6 Mathematical Modeling.....	9
2.6.1 Bounded Johnson Distribution.....	11
2.6.2 Lognormal Johnson Distribution	13
2.6.3 Unbounded Johnson Distribution	13
2.6.4 Chauvenet’s Criterion	14
3.0 SPECIMEN PREPARATION AND TEST PROCEDURE	15
4.0 RESULTS	17
4.1 Determining the Appropriate Johnson Distribution.....	17
4.2 Chauvenet’s Criterion	19
4.3 Bounded Johnson Distribution.....	20
4.4 Lognormal Johnson Distribution	21
4.5 Unbounded Johnson Distribution	22
4.6 Distribution Parameters	24

5.0	CONCLUSIONS AND RECOMMENDATIONS	28
6.0	REFERENCES	30
	APPENDIX A.....	32
A.1	Hit Delay Time	33
A.2	Peak Detection Time.....	33
A.3	Hit Lockout Time.....	34
	APPENDIX B.....	35

LIST OF TABLES

	Page
Table 2.1 Counts, Mechanism 2	12
Table 4.1 Table of Best Fit Johnson Distributions	17
Table 4.2 Table of Acceptable Standard Deviations	20
Table 4.3 Risetime Parameters	25
Table 4.4 Counts Parameters	25
Table 4.5 Energy Parameters	25
Table 4.6 Duration Parameters	26
Table 4.7 Amplitude Parameters.....	26
Table 4.8 Counts to Peak Parameters	26
Table 4.9 Table of Distribution Shape Parameters	27

LIST OF FIGURES

	Page
Figure 2.1 AE Signal Parameters.....	4
Figure 2.2 Unsorted Amplitude Distribution.....	7
Figure 2.3 Sorted AE Data Plot.....	8
Figure 2.4 Sorted Amplitude Distributions.....	9
Figure 2.5 $\beta_1 - \beta_2$ Plot.....	11
Figure 4.1 $\beta_1 - \beta_2$ Plot with Data Sorted by Failure Mechanism	18
Figure 4.2 $\beta_1 - \beta_2$ Plot with Data Sorted by AE Parameter.....	19
Figure 4.6 Lognormal Johnson Fit for the Energy Distribution, Mechanism 2.....	22
Figure 4.7 Lognormal Johnson Fit for the Duration Distribution, Mechanism 2	22
Figure 4.8 Unbounded Johnson Fit for the Amplitude Distribution, Mechanism 2	23
Figure 4.9 Unbounded Johnson Fit for the Amplitude Distribution, Mechanism 5	23
Figure 4.10 Bounded Johnson Fit for the Amplitude Distribution, Mechanism 2	24
Figure 4.11 Bounded Johnson Fit for the Amplitude Distribution, Mechanism 5	24
Figure A.1 Illustration of the HDT Parameter	33
Figure A.2 Illustration of PDT Parameter.....	34
Figure A.3 Illustration of HLT Parameter	34
Figure B.1 Bounded Johnson Fit for the Rise Time Distribution, Mechanism 1	36
Figure B.2 Bounded Johnson Fit for the Counts Distribution, Mechanism 1	36
Figure B.3 Lognormal Johnson Fit for the Energy Distribution, Mechanism 1	36
Figure B.4 Bounded Johnson Fit for the Duration Distribution, Mechanism 1.....	37
Figure B.5 Bounded Johnson Fit for the Amplitude Distribution, Mechanism 1.....	37
Figure B.6 Bounded Johnson Fit for the Counts to Peak Distribution, Mechanism 1.....	37
Figure B.7 Bounded Johnson Fit for the Rise Time Distribution, Mechanism 2	38
Figure B.8 Bounded Johnson Fit for the Counts Distribution, Mechanism 2	38
Figure B.9 Lognormal Johnson Fit for the Energy Distribution, Mechanism 2.....	38
Figure B.10 Lognormal Johnson Fit for the Duration Distribution, Mechanism 2	39
Figure B.11 Unbounded Johnson Fit for the Amplitude Distribution, Mechanism 2.....	39

Figure B.12	Bounded Johnson Fit for the Counts to Peak Distribution, Mechanism 2...	39
Figure B.13	Bounded Johnson Fit for the Rise Time Distribution, Mechanism 3	40
Figure B.14	Lognormal Johnson Fit for the Counts Distribution, Mechanism 3	40
Figure B.15	Lognormal Johnson Fit for the Energy Distribution, Mechanism 3	40
Figure B.16	Lognormal Johnson Fit for the Duration Distribution, Mechanism 3	41
Figure B.17	Lognormal Johnson Fit for the Amplitude Distribution, Mechanism 3	41
Figure B.18	Bounded Johnson Fit for the Counts to Peak Distribution, Mechanism 3...	41
Figure B.19	Bounded Johnson Fit for the Rise Time Distribution, Mechanism 4	42
Figure B.20	Lognormal Johnson Fit for the Counts Distribution, Mechanism 4	42
Figure B.21	Bounded Johnson Fit for the Energy Distribution, Mechanism 4	42
Figure B.22	Bounded Johnson Fit for the Duration Distribution, Mechanism 4.....	43
Figure B.23	Lognormal Johnson Fit for the Amplitude Distribution, Mechanism 4	43
Figure B.24	Bounded Johnson Fit for the Counts to Peak Distribution, Mechanism 4...	43
Figure B.25	Lognormal Johnson Fit for the Rise Time Distribution, Mechanism 5	44
Figure B.26	Bounded Johnson Fit for the Counts Distribution, Mechanism 5.....	44
Figure B.27	Bounded Johnson Fit for the Energy Distribution, Mechanism 5	44
Figure B.28	Bounded Johnson Fit for the Duration Distribution, Mechanism 5.....	45
Figure B.29	Unbounded Johnson Fit for the Amplitude Distribution, Mechanism 5.....	45
Figure B.30	Bounded Johnson Fit for the Counts to Peak Distribution, Mechanism.....	45

1.0 INTRODUCTION

1.1 Overview

Acoustic emission (AE) is a unique form of nondestructive testing. It is a passive technique that does not actively send out a signal into the material and then listen for a return echo; rather, AE detects the sound waves that are generated within a specimen that is under a load. This means that the specimen must be under a load in order for a signal to be generated. The major advantage of AE testing is that it is a dynamic test. What this means is that data can be taken in service, in real time, and the results of the test are immediately known. A widely used technique in industry, AE has been employed in such diverse applications as pressure vessel proof testing, in-flight monitoring of fatigue cracking in aircraft, and prediction of ultimate strengths/loads in composite structures.

The basis of this thesis is to mathematically model the AE flaw growth data that is generated from a tensile test. It will be shown that the various histogram plots of the AE parameters for the flaw growth data can be successfully modeled using Johnson distributions. It is anticipated that the shape and scale parameters associated with these distribution curves will provide the input for future ultimate strength/load prediction schemes.

1.2 Previous Research

Previous research has shown that AE data can be used to create a prediction model for ultimate strength/load in several different applications. Fisher and Hill [1] found that by using a back propagation neural network based on the percentage of hits in each of the failure mechanisms, it was possible to create a burst pressure model for a filament wound fiberglass/epoxy pressure vessel. Walker and Hill [2] were also able to use a back propagation neural network based on the Weibull distribution shape and scale parameters to create an ultimate load prediction model for graphite/epoxy tensile test specimens.

Previous research has also shown that AE data can be sorted into the different failure mechanisms for composites. Ely and Hill [3] found that in a carbon fiber reinforced composite the different failure mechanisms could be sorted out by analyzing the amplitude versus duration or amplitude versus rise time plots. While this technique was useful for a test consisting of a relatively small data set, it is not as useful when extensive overlap exists between the failure mechanism distributions. Kouvarakos and Hill [4] used an iterative approach to isolate the different failure mechanisms. Their iterative approach employed the duration of the signal as the main sorting parameter. This technique sorted the data into six different failure mechanisms plus ultimate specimen failure.

Previous research has also shown that AE data can be fit by several different curves. One of the first distributions used was the extreme value distribution. This was used by Graham [5] to fit the amplitude distributions of the four failure mechanisms from a composite beam. Another distribution that has been used is the lognormal distribution. Pollock [6] suggested this for modeling amplitude distributions. Kouvarakos and Hill [4] found that most of the AE amplitude distributions in a fiberglass/epoxy tensile test specimen could be fit by the normal or Gaussian distribution, but that because of the threshold, the lowest distribution is skewed to the right; therefore it was best fit by either a lognormal or extreme value distribution.

Hill and Demeski [7] demonstrated that a neural network could be used to quickly and accurately classify AE data. Using a Kohonen self-organizing map (SOM), they more accurately classified the hand edited data of Kouvarakos and Hill [4] into five separate failure mechanisms – instead of the original six – plus ultimate failure. After the neural network sorted the data, they were able to mathematically model the data using three distributions: normal, extreme value, and lognormal. However, since the normal and extreme value distributions are specialized cases of the lognormal distribution, the lognormal was proposed as the best fit model.

1.3 Current Approach

While previous research has shown that it is possible to create an ultimate strength/load prediction model for various types of specimens, several different approaches were employed. This research is being conducted to try to find a mathematical approach that can be used for all types of data. If this can be found, then the steps taken to create a prediction model might be simplified and standardized. As seen in Hill and Demeski's [7] work, several types of distributions can be used for modeling the data. The basis of this work was to find a single distribution type that could be used to accurately model all of the AE parameter data. Johnson distributions are known to fit many different shapes. Because of this, the three different Johnson distributions were used to fit all the data herein.

2.0 THEORY

2.1 Acoustic Emission

Acoustic emissions (AE) are defined as the elastic waves generated by the rapid release of energy from sources within a material under an applied load. A piezoelectric sensor attached to the specimen detects these stress waves and converts them into a voltage versus time waveform. The sensor output is then connected to various amplifiers and filters before being sent to a data acquisition system, where the AE signal is quantified

2.2 AE Signal Parameters

The AE system generates six quantification parameters from the signal as shown in Figure 2.1. A voltage threshold is set to help eliminate any background noise. The system does not register a hit until the incoming signal crosses the threshold voltage. Once a hit has been detected, the system begins quantifying the signal. The hit ends once the signal no longer crosses the threshold. The six parameters that are quantified are as follows:

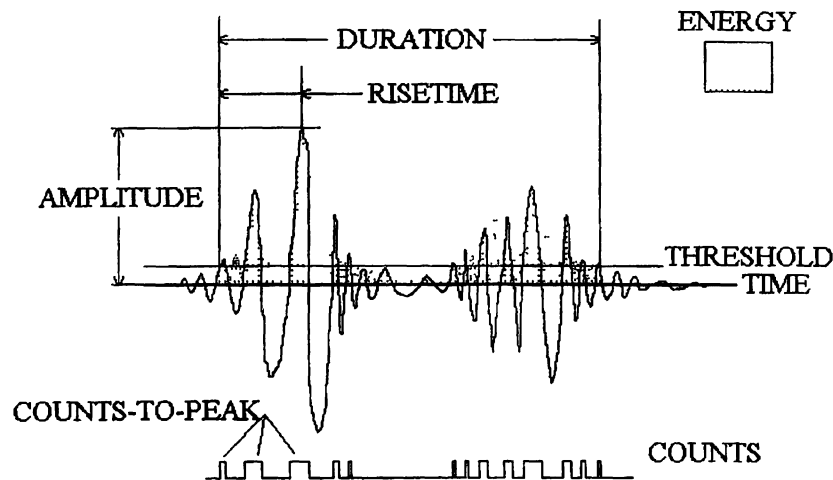


Figure 2.1 AE Signal Parameters

Counts:	The total number of times that the signal crosses the threshold.
Counts to Peak:	The number of counts to reach the peak amplitude of the signal.
Amplitude:	The peak value of the signal voltage measured in decibels (dB).
Duration:	The total amount of time that the signal is above the threshold, measured in microseconds (μs).
Energy:	The area under the rectified signal, measured in energy counts.
Rise time:	The time, from the start of the event to the peak amplitude, measured in microseconds (μs).

2.3 Initial Settings

Before a test can be run, the data acquisition system must have various settings entered into it. The purpose of these settings is to make sure that the system will properly detect the signals. These settings include the gain, threshold, and three different timing parameters: hit delay time (HDT), peak detection time (PDT), and hit lockout time (HLT). These timing parameters are explained in Appendix A.

The gain amplifies the signal to a usable level. The smallest detectable signal is the 1.0 microvolt (μV) reference voltage. A typical gain setting before the signal reaches the data acquisition system is 40 dB, which corresponds to a factor of 100 times amplification. To filter out some of the background noise, a threshold is used. The threshold is used to set the minimum voltage that the system will recognize. A typical threshold setting for composites is 40 dB or 0.1 mV. This setting means that the AE analyzer will ignore any signal that is not greater than 40 dB. Threshold settings are found through experimentation, because the background noise levels vary between test locations.

2.4 Composite Failure Mechanisms

Composites typically have five principle failure mechanisms. These are fiber breaks, transverse matrix cracking, fiber/matrix debonding, fiber pullouts, and longitudinal splitting. A brief description of each is given below.

Fiber breaks:	The mechanism in which the fiber actually breaks
Transverse matrix cracking:	The mechanism in which the matrix cracks normal to the fiber direction.
Fiber/matrix debonding:	The process in which the fibers separate from the matrix.
Fiber pullouts:	The mechanism in which the fiber is pulled out of the matrix material.
Longitudinal splitting	The mechanism in which the matrix cracks along the fiber direction.

2.5 Classification of Failure Mechanisms

The unsorted amplitude distribution for the tensile test does not appear to have any distinguishable failure mechanism humps, as can be seen in Figure 2.2 [4]. This is due to the large number of data points (21,966 AE hits) that were obtained during the test. Although the threshold is set to 40 dB, due to the nature of the system, some data are taken below the threshold.

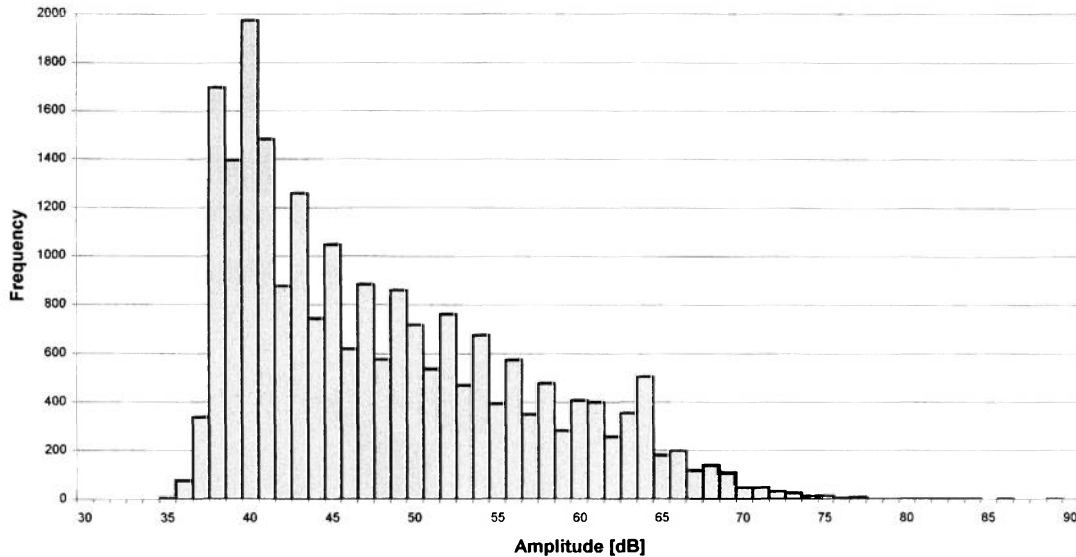


Figure 2.2 Unsorted Amplitude Distribution

When this many data points are obtained, there tends to be considerable overlap in the amplitude bands associated with each failure mechanism, making it virtually impossible to sort by hand. Because of this, a classification neural network was introduced for sorting the data. A neural network works similar to the human brain. It processes data in parallel, using multiple inputs to arrive at the correct classification.

A Kohonen self-organizing map (SOM) was previously used by Hill and Demeski [7] to sort the tensile test data used in this work. This network has three layers, the input layer, the hidden (processing) layer, and the output layer. The layers are connected with adjustable weights. The network takes the input data, runs it through the processing layer, and then assigns it an x-y output. This x-y value is nondimensional and is used strictly for mapping. A plot of the x-y outputs reveals the beginnings of clusters. The network runs iteratively, adjusting the connection weights until all the data is grouped. The network is considered to be trained when, after numerous iterations, the connection weights either no longer change or the change is minimal. On mapping the x-y outputs, failure mechanism clusters appear.

Here, the input for the SOM neural network was the six AE parameters for each AE hit. The SOM looks at the six parameters for each data point and tries to place it near similar data points. It can be seen in Figure 2.3 that the neural network sorted the data into five clusters, each representing a different composite failure mechanism. Figure 2.3 is representative of the x-y output produced by the SOM from the Neuralworks Pro II Plus software package by Neuralware.

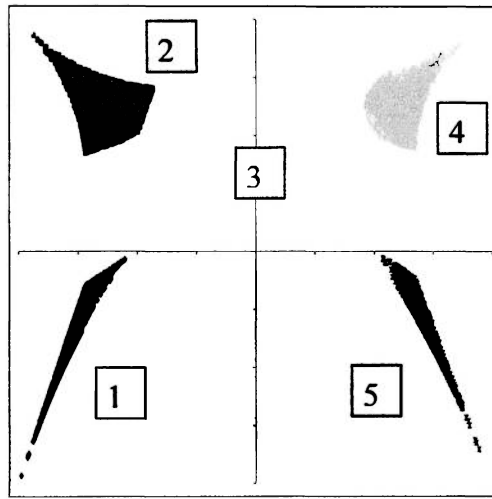


Figure 2.3 Sorted AE Data Plot

Figure 2.4 shows the relative frequency plots of the five sorted mechanisms. It can be seen that there is a significant amount of overlap between the mechanisms, with mechanism 3 being hidden in between mechanisms 2 and 4.

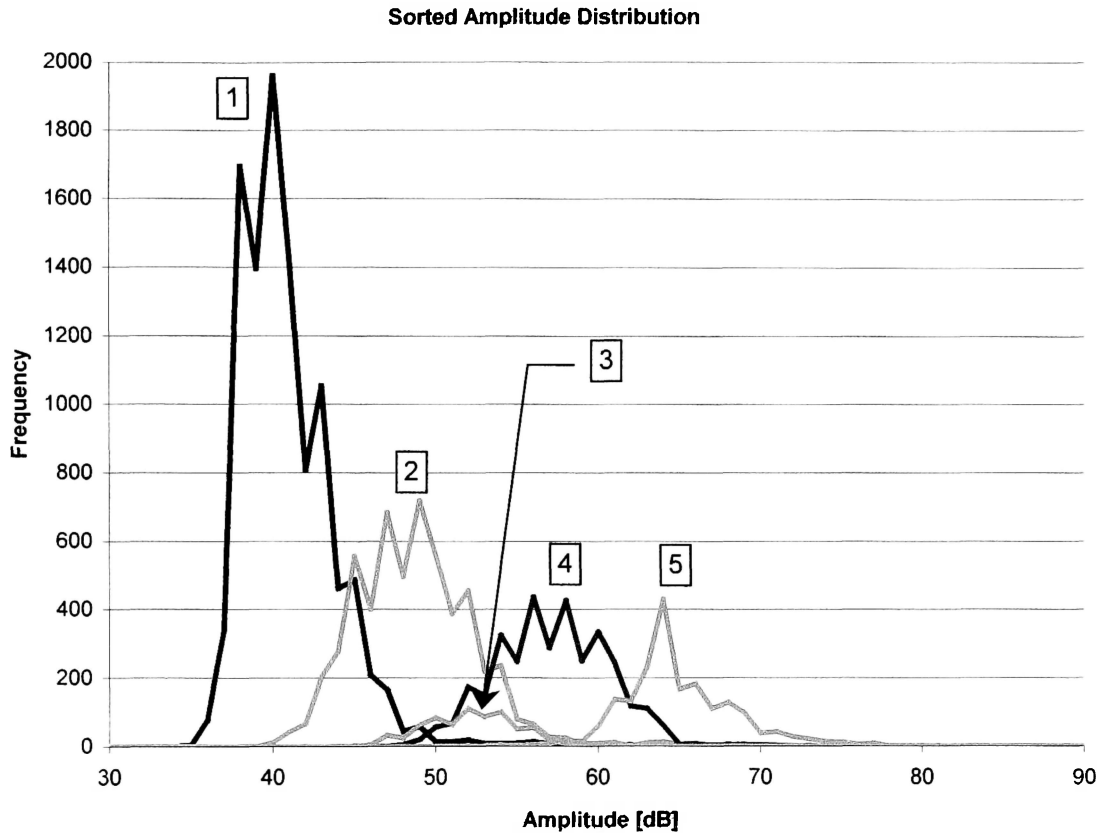


Figure 2.4 Sorted Amplitude Distributions

2.6 Mathematical Modeling

The most versatile of all the statistical distribution types is the Johnson distribution [8]. All of the previously mentioned distributions are specialized cases of the three types of Johnson distributions. The first step in determining which type of Johnson distribution – bounded, lognormal, or unbounded – provides the best fit to a given set of data is to calculate the mean μ , standard deviation σ , and the second, third, and fourth moments of the distribution:

$$m_2 = \frac{1}{n} \sum_{i=1}^n (x_i - \mu)^2 = \sigma^2$$

$$m_3 = \frac{1}{n} \sum_{i=1}^n (x_i - \mu)^3$$

and

$$m_4 = \frac{1}{n} \sum_{i=1}^n (x_i - \mu)^4 .$$

Then determine the relative skewness from the expression

$$\sqrt{\beta_1} = \frac{m_3}{(m_2)^{3/2}}$$

and the relative kurtosis or peakedness from

$$\beta_2 = \frac{m_4}{(m_2)^2} .$$

Finally, the relative skewness is squared to obtain β_1 , which is then plotted along with β_2 on a β_1 - β_2 plot as shown in Figure 2.5. Here since the point (β_1, β_2) lies close to lognormal Johnson S_L line, the data curve is best modeled as a lognormal distribution. Points that plot in between the lognormal and the impossible lines are best fit as the bounded Johnson S_B distribution. Whereas those data whose (β_1, β_2) values fall below the lognormal line are best fit as unbounded Johnson S_U distributions.

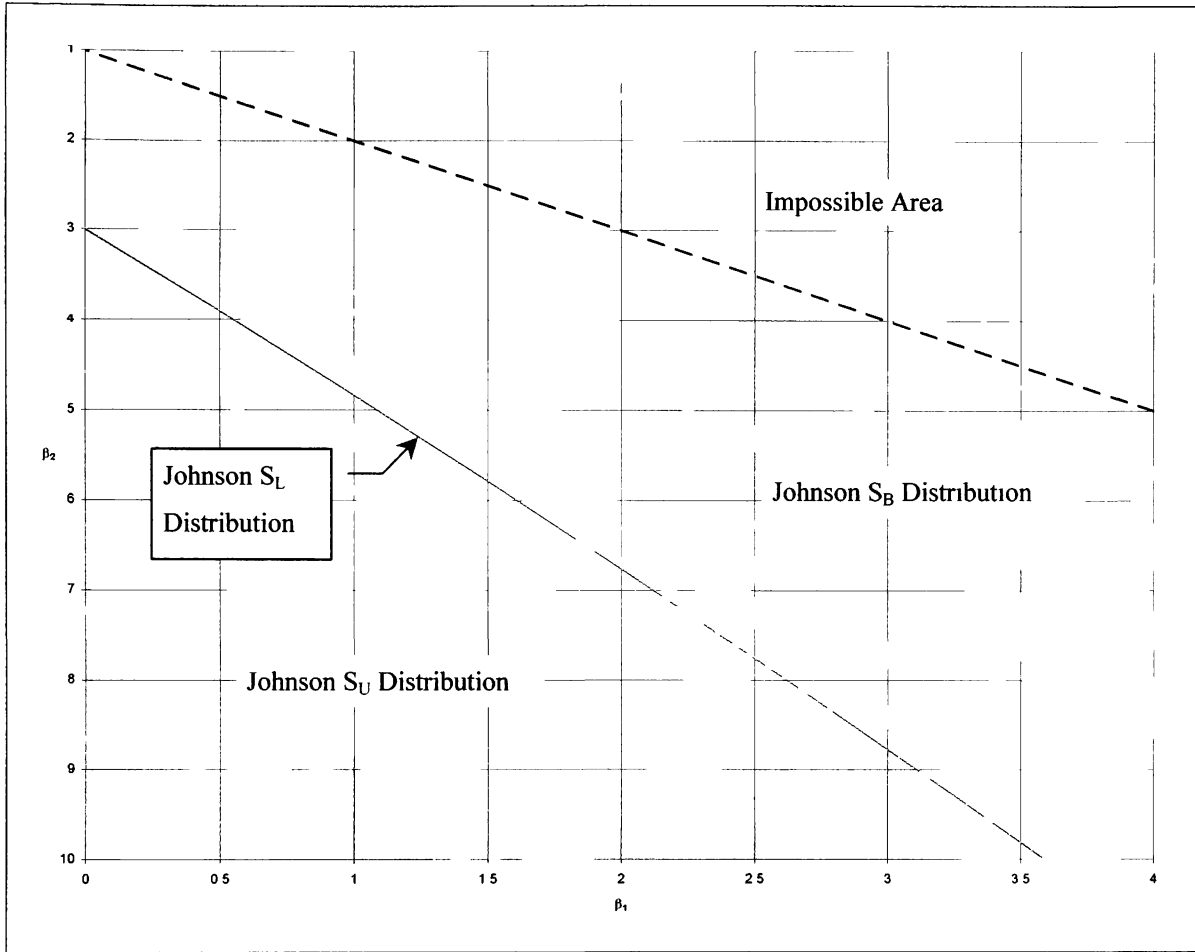


Figure 2.5 $\beta_1 - \beta_2$ Plot

2.6.1 Bounded Johnson Distribution

The equation for the probability density function of the bounded Johnson distribution [8] is given as

$$f_{S_B}(x) = \frac{\eta}{\sqrt{2\pi}} \frac{\lambda}{(x - \varepsilon)(\lambda - x + \varepsilon)} \exp \left\{ -\frac{1}{2} \left[\gamma + \eta \ln \left(\frac{x - \varepsilon}{\lambda - x + \varepsilon} \right) \right]^2 \right\},$$

where

$$\eta = \frac{Z_{1-\alpha'} - Z_\alpha}{\ln \left[\frac{(x_{1-\alpha'} - \varepsilon)(\varepsilon + \lambda - x_\alpha)}{(x_\alpha - \varepsilon)(\varepsilon + \lambda - x_{1-\alpha'})} \right]}$$

and

$$\gamma = z_{1-\alpha'} - \eta \ln \left(\frac{x_{1-\alpha'} - \epsilon}{\epsilon + \lambda - x_{1-\alpha'}} \right)$$

are the two shape parameters. Here x is the AE parameter value (counts, amplitude, energy, etc.), ϵ is the minimum value of the variate x , and $\epsilon + \lambda$ is the maximum value of x for the data set. The values z_α and $z_{1-\alpha'}$ correspond to the α and $(1 - \alpha')$ percentiles of the standard normal distribution; whereas x_α and $x_{1-\alpha'}$ are the corresponding x values for those data percentiles. To fit this data it was decided to fit the 9th and 91st percentile data points. This resulted in $z_{0.09}$ and $z_{0.91}$ being equal to 1.34.

Table 2.1 is an example data set where $x_{0.09}$ and $x_{0.91}$ are the 508th and 5139th data points. This leads to $x_{0.09}$ and $x_{0.91}$ being 1 and 4 respectively.

Table 2.1 Counts, Mechanism 2

Counts	Frequency	Cumulative Frequency
0	11	11
1	597	608
2	2689	3297
3	1667	4964
4	578	5542
5	86	5628
6	19	5647

The following steps are taken to fit the Johnson S_B distribution: (1) having determined from the $\beta_1 - \beta_2$ plot that the S_B distribution is the appropriate distribution, (2) estimate the shape, location, and scale parameters (γ , η , ϵ , and λ respectively), then (3) calculate and plot the expected frequencies for the fitted distribution from the equation

$$P(x) = nwf(x)$$

with

$$n = \text{number of AE hits in the data set}$$

w = width of the histogram intervals.

2.6.2 Lognormal Johnson Distribution

The equation for the lognormal probability density distribution is [8]

$$f_{S_L}(x) = \frac{\eta}{\sqrt{2\pi}} \frac{\lambda}{(x - \varepsilon)(\lambda - x + \varepsilon)} e^{-\frac{1}{2} \left[\gamma + \eta \ln \left(\frac{x - \varepsilon}{\lambda - x + \varepsilon} \right) \right]^2},$$

where

$$\eta = \frac{1}{\sigma}$$

and

$$\gamma = -\frac{\mu}{\sigma}$$

with

μ and σ again being the mean and standard deviation of each data set.

The following steps are taken to fit the Johnson S_L distribution: (1) determine that the S_L distribution is the appropriate distribution from the $\beta_1 - \beta_2$ plot, (2) estimate the shape, location, and scale parameters (γ , η , ε , and λ respectively), then (3) calculate and plot the expected frequencies $P(x)$ for the fitted distribution.

2.6.3 Unbounded Johnson Distribution

The unbounded Johnson probability density distribution is as follows [8]:

$$f_{S_U}(x) = \frac{\eta}{\sqrt{2\pi}} \frac{1}{\sqrt{(x - \varepsilon)^2 + \lambda^2}} e^{-\frac{1}{2} \left[\gamma + \eta \ln \left\{ \left(\frac{x - \varepsilon}{\lambda} \right) + \left[\left(\frac{x - \varepsilon}{\lambda} \right)^2 + 1 \right]^{1/2} \right\} \right]^2},$$

where

$$\lambda = \frac{\sigma}{\left[\frac{1}{2} (\omega - 1) \left(\omega \cosh \left(2 \frac{\gamma}{\eta} \right) + 1 \right) \right]^{1/2}}$$

and

$$\varepsilon = \mu + \lambda \omega^{\frac{1}{2}} \sinh\left(\frac{\gamma}{\eta}\right)$$

with

$$\omega = e^{\frac{1}{\eta^2}}.$$

The following steps are taken to fit the Johnson S_U distribution: (1) determine that the S_U distribution is the appropriate distribution from the $\beta_1 - \beta_2$ plot, (2) estimate the shape parameters (γ and η) by looking up the $\sqrt{\beta_1}$ and β_2 values for the distribution from Table V (Hahn and Shapiro [8]), (3) calculate ω , (4) determine the scale parameters (ε and λ , respectively), and (5) calculate and plot the expected frequencies $P(x)$.

2.6.4 Chauvenet's Criterion

In all real world testing applications, erroneous data points sometimes make it into a data set. In order to see if there were any bad data points, Chauvenet's criterion [9] was applied to each of the five data sets. Chauvenet's criterion is a mathematical method for analyzing the data set to see if any data points fall outside of an acceptable range and therefore can be eliminated. To apply this criterion, the mean μ and standard deviation σ of the data set are first calculated. The next step is to calculate the ratio of the deviation of each data point from the standard deviation. This value is then compared to the ratio of maximum acceptable deviation to standard deviation. The equation for calculating the maximum acceptable probability is

$$P(z) \leq 1 - \frac{1}{2n},$$

where

n = number of data points.

After $P(z)$ is calculated, the value for the number of standard deviations z that corresponds to this maximum $P(z)$ value is found from the area under the standard normal distribution curve (Table I, Hahn and Shapiro [8]).

3.0 SPECIMEN PREPARATION AND TEST PROCEDURE

One tensile test specimen was used for this test. The test specimen was an eight-layer unidirectional fiberglass/epoxy laminate made in compliance with the ASTM D-3039 standard [4,10]. The fibers were Owens-Corning S-2 glass with the Hexcel Epolite 2410 resin system and 2183 hardener. Aluminum tabs were bonded to both ends of the specimens to prevent crushing/damaging during the test. Without the tabs, the ends of the specimens would have been crushed by the hydraulic grips of the MTS tensile test machine, resulting in extraneous AE data and possibly rendering the analysis useless.

The tensile test was performed using a Physical Acoustics Corporation (PAC) R15 (150 kHz) piezoelectric transducer. The transducer was placed on the center of the specimen, and it was coupled to the specimen using SAE 30 oil and secured with electrical tape. The oil provides acoustical coupling between the sensor and the specimen. Connected to the transducer was a PAC model 1220A preamplifier/filter with a 100 to 300 kHz band pass filter and set for 40 dB (100x) of amplification before the signal is sent to the acoustic emission data analyzer. The AE analyzer used was a PAC LOCAN-AT system. Further amplification may occur within the analyzer, plus it contains the circuitry to quantify, store, and analyze the AE parameter data. The LOCAN-AT hardware settings were as follows:

Gain:	20 dB
Threshold:	40 dB
PDT:	40 μ s
HDT:	150 μ s
HLT:	30 μ s.

Testing was performed at Embry-Riddle Aeronautical University (ERAU) using a 10 kip MTS tensile test machine. The specimen was placed in the MTS machine with a grip pressure of 1400 psi and was loaded in tension along the fiber direction at a rate of

approximately 500 lb/min. The load rate must be chosen such that the AE data acquisition system is not overloaded, at which point it is unable to distinguish one hit from another. The other consideration is that if the load rate is too slow, the test will take an unreasonable amount of time to complete. AE data were taken from the onset of loading to specimen failure. However, the ultimate failure AE data were not included in the modeling effort since these hits occur so quickly that they overlap into multiple hits, which again confuses the analysis process.

4.0 RESULTS

4.1 Determining the Appropriate Johnson Distribution

Figure 4.1 and Figure 4.2 show the locations on the β_1 and β_2 plane where the sorted AE data fell for this test. It can be seen that nineteen of the thirty (β_1, β_2) points lie between the lognormal S_L distribution line and the impossible line. This says that these data are best fit by the bounded Johnson S_B distribution. For the nine (β_1, β_2) points that plot relatively close to the lognormal line, the lognormal S_L distribution is used to fit the data. Finally, for the remaining two (β_1, β_2) points that fall below the line, the unbounded Johnson S_B distribution is the appropriate model. Table 4.1 shows which Johnson distribution was used for the various mechanisms according to their location on the $\beta_1 - \beta_2$ plane.

Table 4.1 Table of Best Fit Johnson Distributions

Mechanism	Rise Time	Counts	Counts to Peak	Energy	Duration	Amplitude
1	S_B	S_B	S_B	S_L	S_B	S_B
2	S_B	S_B	S_B	S_L	S_L	S_U
3	S_B	S_L	S_B	S_L	S_L	S_L
4	S_B	S_L	S_B	S_B	S_B	S_L
5	S_L	S_B	S_B	S_B	S_B	S_U

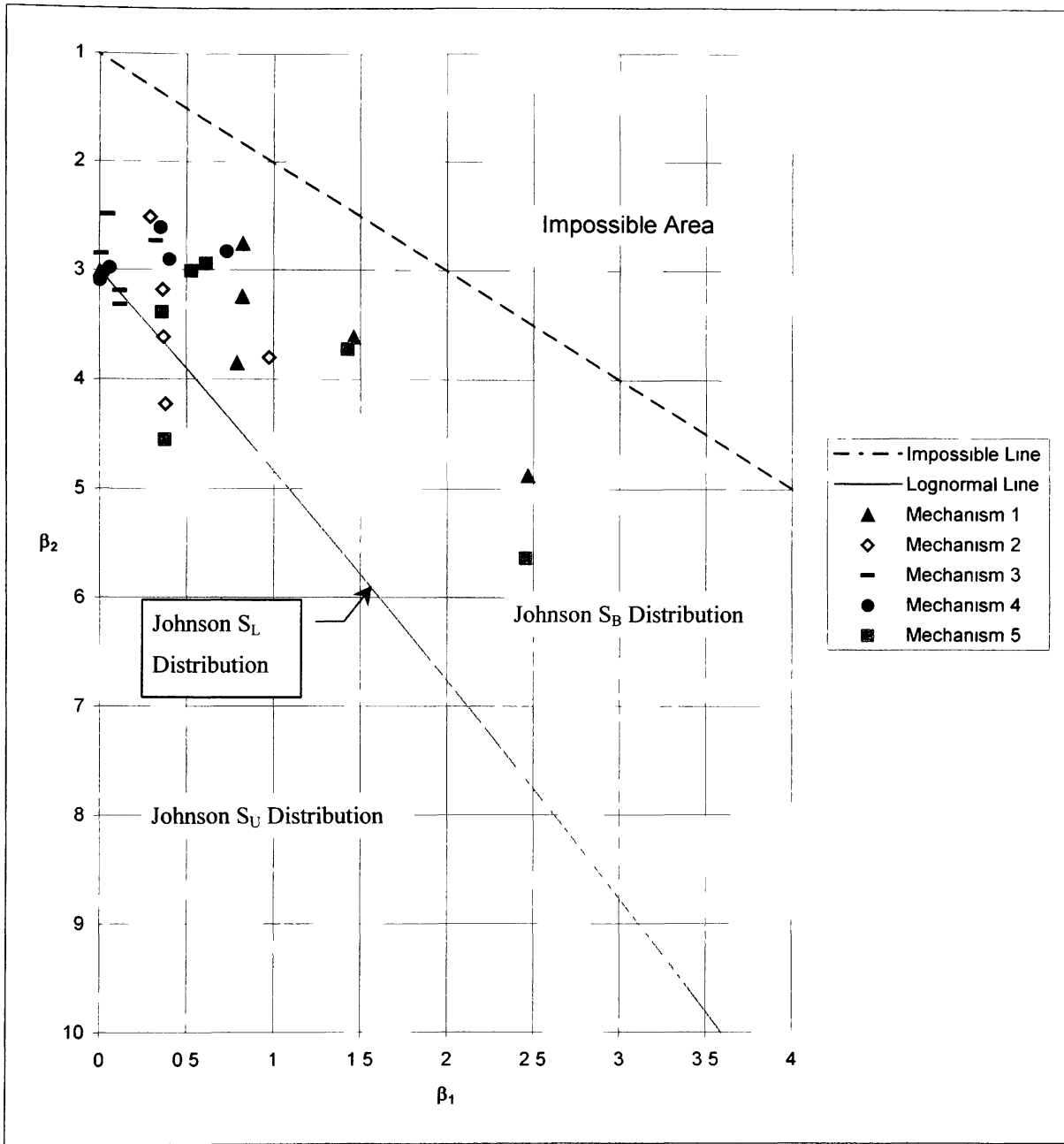


Figure 4.1 $\beta_1 - \beta_2$ Plot with Data Sorted by Failure Mechanism

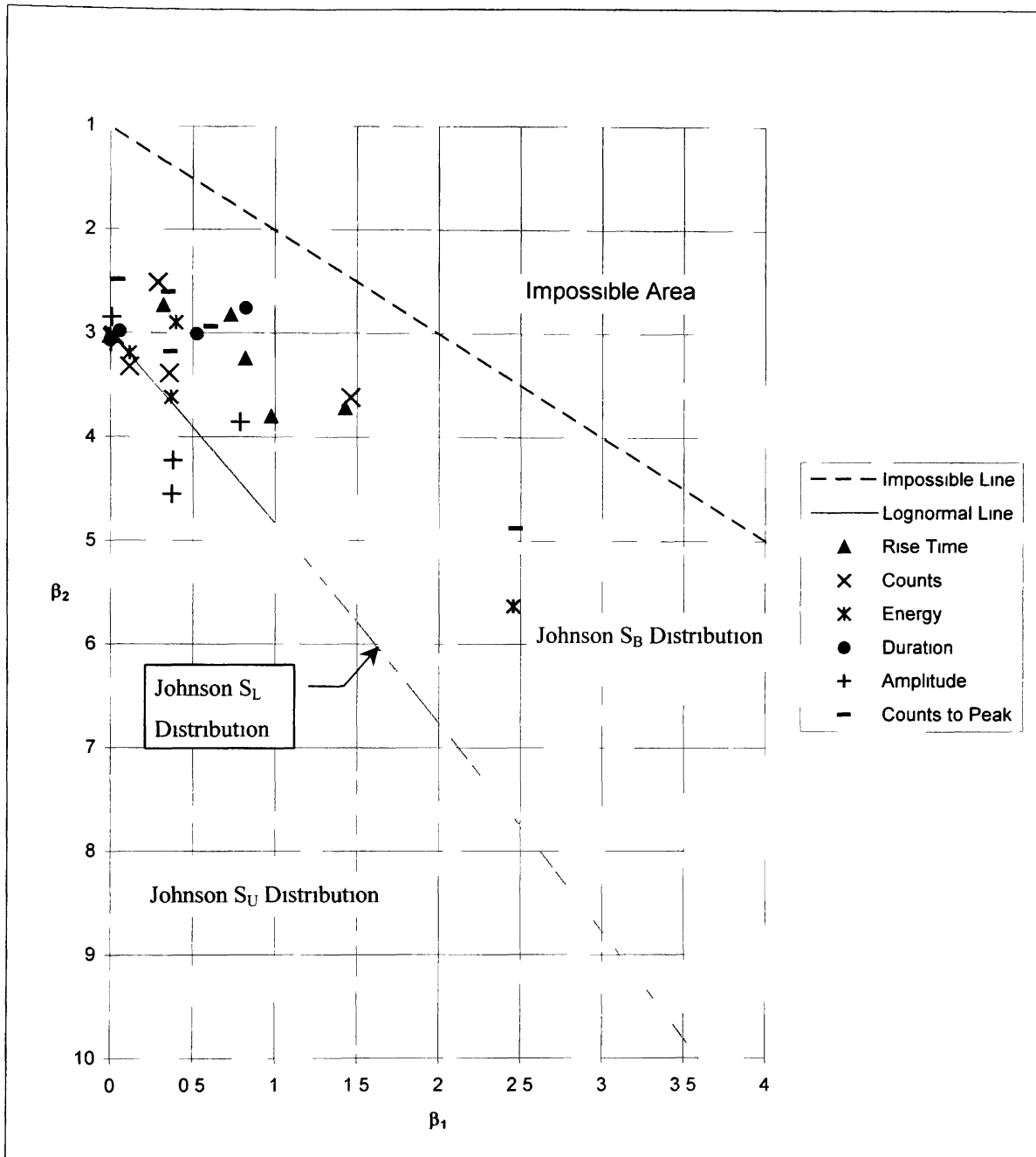


Figure 4.2 $\beta_1 - \beta_2$ Plot with Data Sorted by AE Parameter

4.2 Chauvenet's Criterion

The maximum acceptable standard deviations z were calculated for each mechanism in accordance with Chauvenet's criterion and are summarized in Table 4.2.

Table 4.2 Table of Acceptable Standard Deviations

Mechanism	1	2	3	4	5
n	10,302	5,649	723	3,369	1,923
z	3.82	3.76	3.35	3.68	3.59

If any data point was found to be more than the acceptable number of standard deviations to the left or right of the mean, it was eliminated from the data set as an outlier. One could also put the outliers into the next mechanism to see if they fit there; however this was not done here. After Chauvenet’s criterion was applied to all of the data sets, curve fitting was accomplished using the three different Johnson distributions.

4.3 Bounded Johnson Distribution

Nineteen of the thirty distributions (six AE parameters for each of the five failure mechanisms) were found to be best fit by the bounded Johnson S_B distribution. Figure 4.3 through Figure 4.5 show how well the bounded Johnson distribution fits the various AE parameter distributions for failure mechanism 2. All nineteen of the bounded Johnson S_B distributions are included in Appendix B.

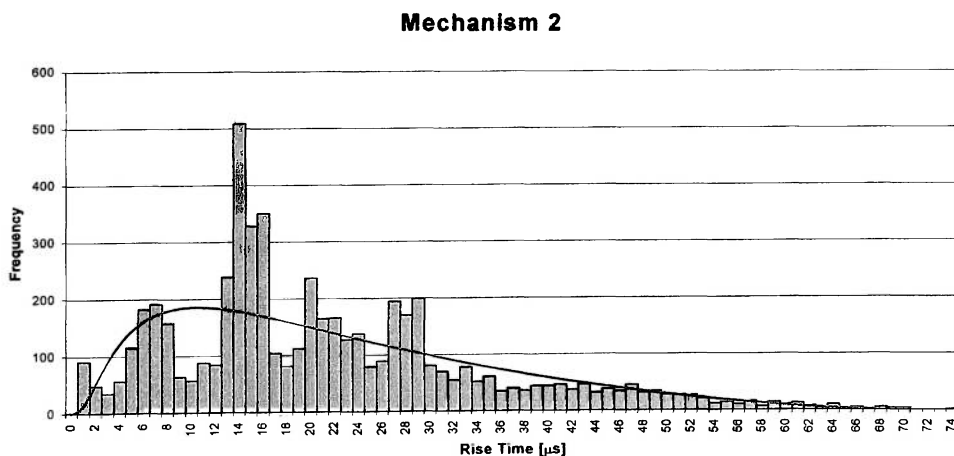


Figure 4.3 Bounded Johnson Fit for the Rise Time Distribution, Mechanism 2

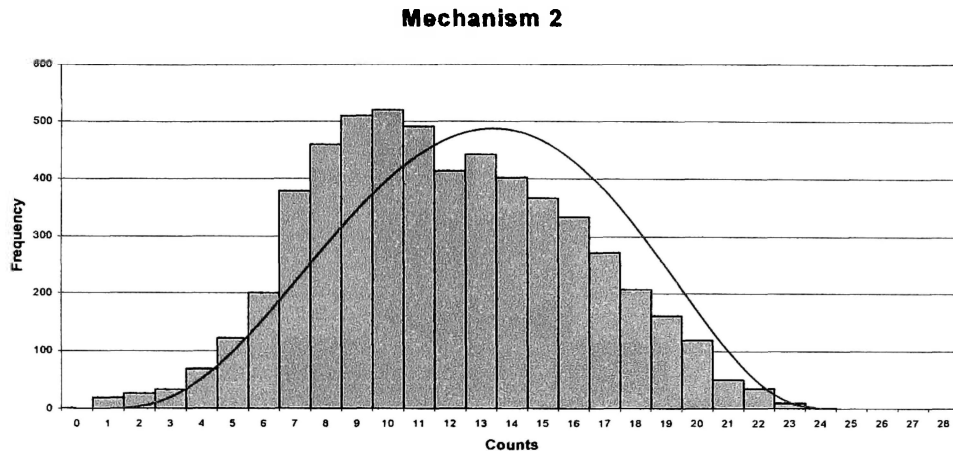


Figure 4.4 Bounded Johnson Fit for the Counts Distribution, Mechanism 2

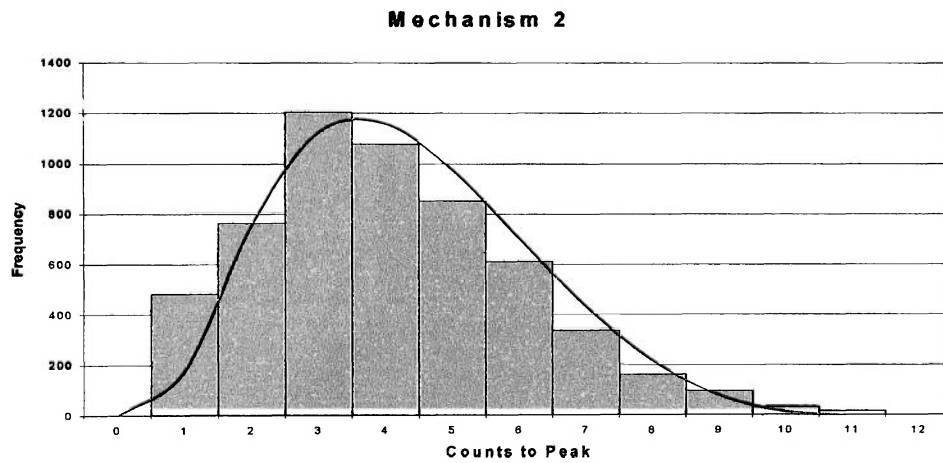


Figure 4.5 Bounded Johnson Fit for the Counts to Peak Distribution, Mechanism 2

4.4 Lognormal Johnson Distribution

Nine of the data sets were shown to be best fit by the lognormal Johnson S_L distribution. Figure 4.6 and Figure 4.7 show lognormal Johnson distribution fits for failure mechanism 2. All nine of the lognormal Johnson S_L fits can be found in Appendix B.

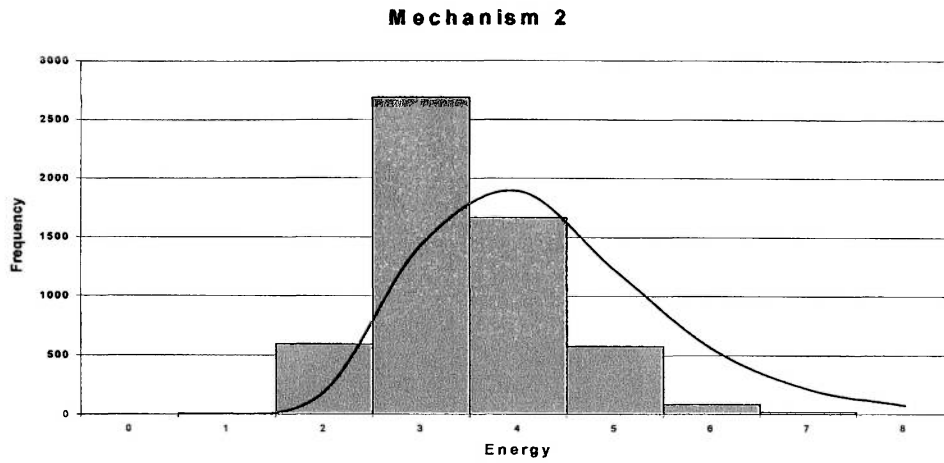


Figure 4.6 Lognormal Johnson Fit for the Energy Distribution, Mechanism 2

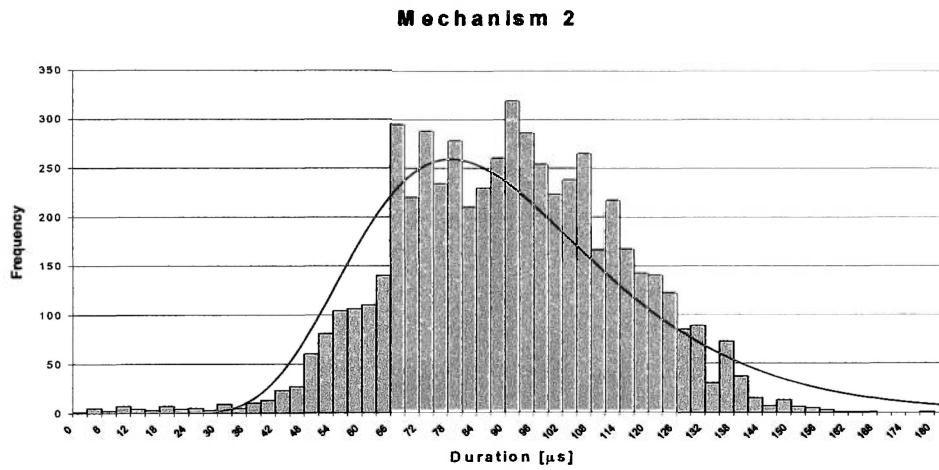


Figure 4.7 Lognormal Johnson Fit for the Duration Distribution, Mechanism 2

4.5 Unbounded Johnson Distribution

Two of the data sets were shown to be best fit by the unbounded Johnson S_U distribution. Figure 4.8 and Figure 4.9 are the amplitude distributions for mechanism 2 and 5 that were fit by the unbounded Johnson distribution.

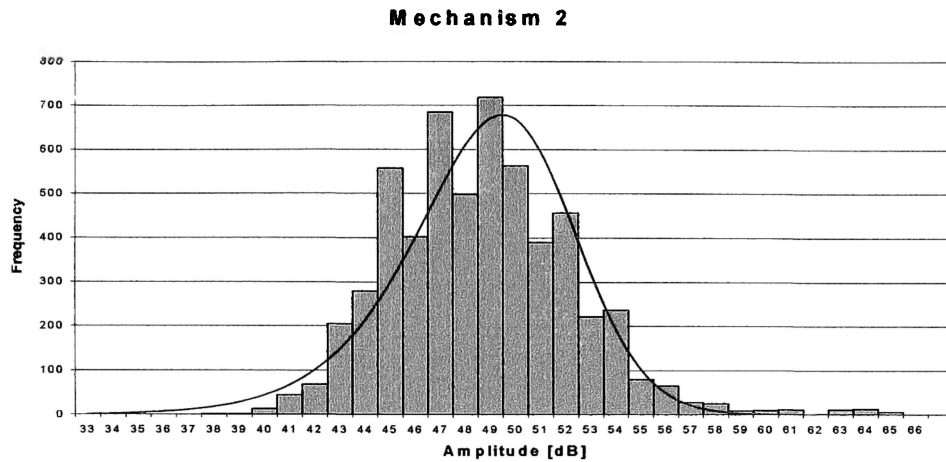


Figure 4.8 Unbounded Johnson Fit for the Amplitude Distribution, Mechanism 2

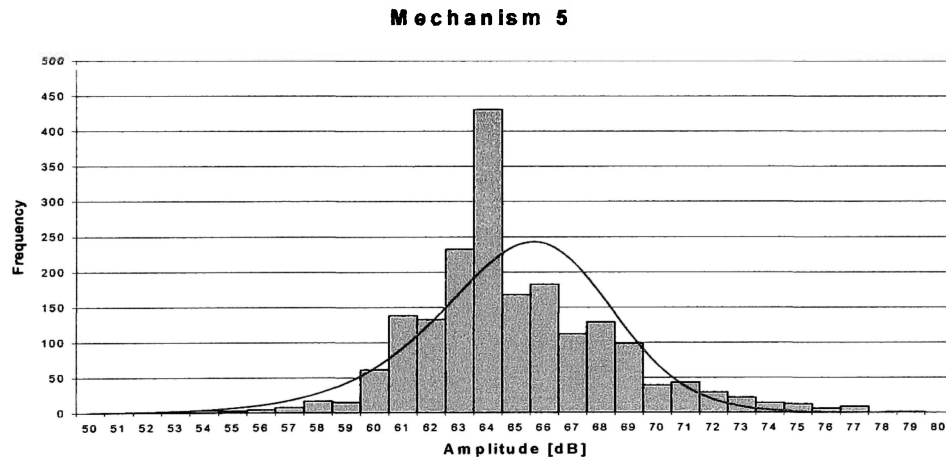


Figure 4.9 Unbounded Johnson Fit for the Amplitude Distribution, Mechanism 5

According to the $\beta_1 - \beta_2$ plot, these two mechanisms are best fit by the unbounded distribution, but they were also fit by the bounded S_B distribution. The bounded fits can be seen in Figure 4.10 and Figure 4.11. It would appear that the bounded S_B distribution fits these distributions as well as the unbounded S_U distribution.

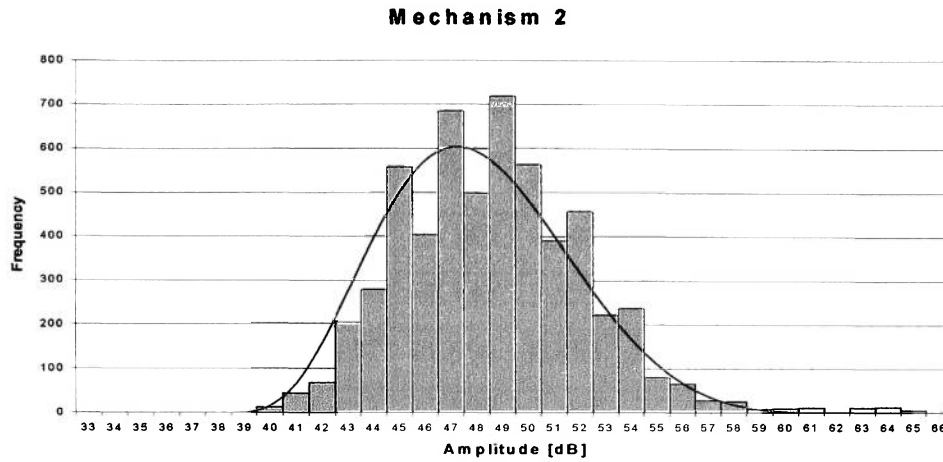


Figure 4.10 Bounded Johnson Fit for the Amplitude Distribution, Mechanism 2

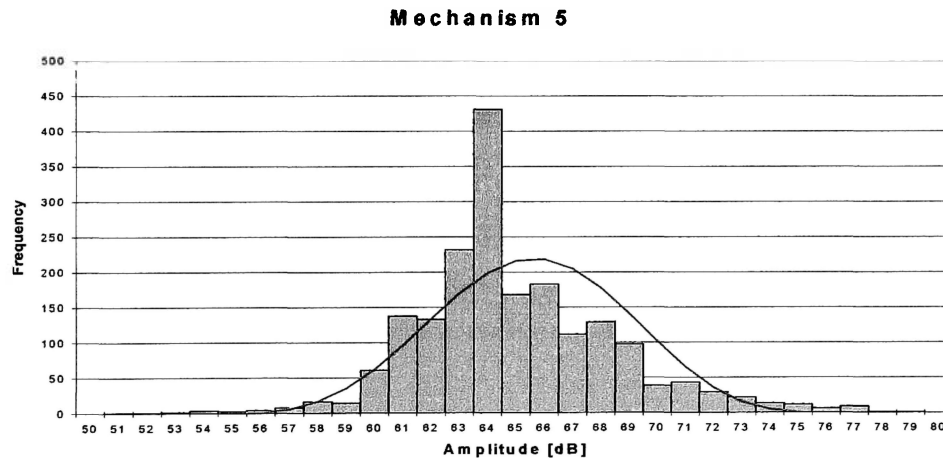


Figure 4.11 Bounded Johnson Fit for the Amplitude Distribution, Mechanism 5

4.6 Distribution Parameters

Table 4.3 through Table 4.8 provide the statistical parameters for all of the Johnson distributions.

Table 4.3 Risetime Parameters

Mechanism	\bar{x}	σ	$\sqrt{\beta_1}$	β_2	ϵ	λ
1	9.941	7.993	0.905	3.246	0	39
2	21.635	13.142	0.987	3.800	0	74
3	35.390	18.143	0.539	2.635	0	91
4	30.237	19.991	0.853	2.798	0	102
5	28.413	17.938	1.194	3.720	0	91

Table 4.4 Counts Parameters

Mechanism	\bar{x}	σ	$\sqrt{\beta_1}$	β_2	ϵ	λ
1	2.471	1.837	1.209	3.616	0	9
2	11.844	4.179	0.171	2.513	0	24
3	18.282	2.993	0.342	3.322	8	27
4	24.779	3.760	0.148	3.024	11	27
5	34.313	5.012	0.629	3.318	17	34

Table 4.5 Energy Parameters

Mechanism	\bar{x}	σ	$\sqrt{\beta_1}$	β_2	ϵ	λ
1	1.868	0.566	0	3.02	0	4
2	2.450	0.898	0.607	3.615	0	7
3	3.758	0.870	0.342	3.194	2	4
4	6.655	2.141	0.634	2.901	0	14
5	18.128	8.700	1.539	5.491	0	54

Table 4.6 Duration Parameters

Mechanism	\bar{x}	σ	$\sqrt{\beta_1}$	β_2	ϵ	λ
1	22.976	21.462	0.907	2.759	0	100
2	89.186	23.242	0.063	3.060	0	177
3	124.891	13.942	0	3.068	78	93
4	160.097	20.450	0.207	2.871	99	135
5	224.212	36.164	0.726	3.008	123	204

Table 4.7 Amplitude Parameters

Mechanism	\bar{x}	σ	$\sqrt{\beta_1}$	β_2	ϵ	λ
1	40.795	2.584	0.888	3.854	35	17
2	48.656	3.613	0.615	4.226	38	27
3	52.112	2.782	0.100	2.849	42	19
4	57.128	3.468	0.028	3.000	44	26
5	64.933	3.497	0.558	4.374	51	28

Table 4.8 Counts to Peak Parameters

Mechanism	\bar{x}	σ	$\sqrt{\beta_1}$	β_2	ϵ	λ
1	1.634	0.962	1.571	4.878	0	5
2	4.064	1.976	0.603	3.183	0	12
3	6.744	2.741	0.218	2.488	0	15
4	6.476	3.532	0.565	2.492	0	18
5	6.453	3.560	0.781	2.939	0	19

The three different types of Johnson distributions (S_B , S_L , and S_U) all have similar shape parameters. The shape parameters for all data sets are found in Table 4.9 below.

Table 4.9 Table of Distribution Shape Parameters

Mechanism	Parameter	Rise Time	Counts	Energy	Duration	Amplitude	Counts to Peak
1	η	0.677	0.967	3.721	0.550	1.413	1.496
	γ	1.124	0.670	5.088	1.172	0.836	0.734
2	η	0.973	1.350	3.381	3.123	2.662	1.377
	γ	1.022	-0.143	4.779	-13.890	1.349	0.877
3	η	1.125	3.105	2.272	2.740	3.161	1.289
	γ	0.485	-7.386	-1.134	-10.395	-7.175	0.447
4	η	0.900	3.448	1.462	1.471	3.367	0.967
	γ	0.872	-9.172	0.000	0.320	-8.535	0.670
5	η	1.506	1.646	1.506	1.351	2.37	1.211
	γ	-4.743	-0.342	0.891	-0.252	0.909	0.687

5.0 CONCLUSIONS AND RECOMMENDATIONS

It was found that, for the most part, the Kohonen SOM neural network was able to successfully sort the AE data into five failure mechanisms. Based on prior experiments that have been done to discover the physical source for each mechanism, mechanism 1 is most likely transverse matrix cracking, while mechanism 5 is probably fiber breaks. It is possible that mechanism 3 is a subset of mechanisms 2 and 4. This may be longitudinal splitting [3]. More testing would be necessary to identify with certainty the sources corresponding to mechanisms 2, 3, and 4.

There were a few outliers (misclassifications) that had to be statistically removed from the failure mechanism clusters. When the (β_1, β_2) values were plotted for the resulting sorted data sets, it was found that nineteen of the curves were within the bounded region of the plot. Two of the curves were within the unbounded region, and the remaining nine curves were on or near the lognormal line. Before the data were given to the SOM neural network, those data associated with ultimate failure of the specimen were supposed to have been removed. When performing this operation on the data, an error may have been made, in that some of the ultimate failure data points were not removed. It is believed that these data may have caused two of the distributions to fall into the unbounded region. Additionally, some of the bounded distributions did not provide as good a fit as was hoped.

Chauvenet's criterion assumes a normal distribution (symmetrical) while most of the data herein are right skewed. This causes the lower end data points to not be removed. It was found that Chauvenet's criterion was not adequate in removing outliers from the data because of the skewness of the data. If the lower end data points were removed from the data set, the bounded Johnson distribution would better fit the data. This is because those particular data points were forcing the fit, decreasing the relative kurtosis or peakedness β_2 of the curve. If a different method had been used to find the outliers, a better fit may have resulted. Values of β_1 and β_2 are very sensitive to outliers; thus incorporation of skewness into the removal of outliers should improve the fit. It is anticipated that this

would result in the two S_U curves becoming S_B curves. It is recommended that any future work incorporate the Chi-squared goodness of fit test to verify the curve fitting results.

Further testing should also be conducted to develop an ultimate strength equation for tensile test specimens. This would require the construction of at least nine ASTM standard tensile test specimens from the same material. The shape parameters of the Johnson distributions (η, γ) could then be used in a multivariate statistical analysis or a back propagation neural network for prediction of ultimate strengths [1,2].

6.0 REFERENCES

1. Fisher, M. E. and Hill, E. v. K., "Burst Pressure Prediction of Filament Wound Composite Pressure Vessels Using Acoustic Emission," MSAE Thesis, 1996, Embry-Riddle Aeronautical University, Daytona Beach, FL.
2. Walker II, J. L. and Hill, E. v. K., "Backpropagation Neural Network for Predicting Ultimate Strengths of Unidirectional Graphite/Epoxy Tensile Specimens," *Advanced Performance Materials*, Vol 3, No. 1, 1996, 75-83.
3. Ely, T. M. and Hill, E. v. K., "Characterization of Failure Mechanisms in Graphite/Epoxy Tensile Test Specimen using Acoustic Emission Data," Proceedings of Fourth International Symposium on Acoustic Emission from Composite Materials (Seattle, WA: American Society for Nondestructive Testing, July 27-32, 1992), 187-199.
4. Kouvarakos, M. and Hill, E. v. K., "Isolating Failure Mechanisms in a Fiberglass/Epoxy Tensile Test Specimen Using Acoustic Emission Signal Parameters," MSAE Thesis, 1992, Embry-Riddle Aeronautical University, Daytona Beach, FL.
5. Graham, L. J., "Acoustic Emission Signal Analysis for Failure Mode Identification," 1980 Paper Summaries, ASNT National Spring Conference, American Society for Nondestructive Testing, Columbus, OH, 1980, 74-79.
6. Pollock, A. A., "Acoustic Emission Amplitude Distributions," International Advances in Nondestructive Testing, Vol. 7, Gordon & Breach, Newark, NJ, 1981, 215-239.

7. Hill, E. v. K. and Demeski, R. J., "Modeling of Acoustic Emission Failure Mechanism Data from a Fiberglass/Epoxy Tensile Test Specimen," AE 699 Paper, Embry-Riddle Aeronautical University, Daytona Beach, FL, 1996.
8. Hahn, G. and Shapiro, S., Statistical Models in Engineering, John Wiley & Sons, Inc., New York, 1994, 195-220
9. Holman, J. P., Experimental Methods for Engineers, McGraw Hill, New York, 2001, 78-80.
10. ASTM Standard D3039-76 (Reapproved 1982), Annual Book of ASTM Standards; reprinted in ASTM Standards and Literature References for Composite Materials, Philadelphia, PA: American Society for Testing Materials, 1987, 39.

APPENDIX A
ACOUSTIC EMISSION TIMING PARAMETERS

A.1 Hit Delay Time

An illustration of hit delay time is shown in Figure A.1. HDT is used to enable the system to detect the end of a hit. The HDT is the amount of time that the system waits when a signal goes below the threshold before it stops recording the hit. If the next signal should cross the threshold before the HDT has passed, the system will recognize it as part of the initial hit. An HDT value of 150 microseconds was used in these tests.

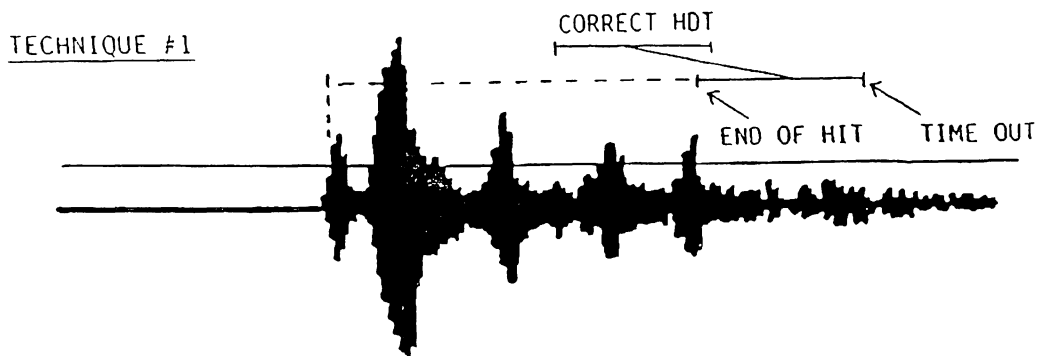


Figure A.1 Illustration of the HDT Parameter

A.2 Peak Detection Time

Peak detection time is the amount of time that the system uses to determine the peak value of the signal. An illustration of PDT is shown in Figure A.2. The PDT value used in these tests was 40 microseconds.

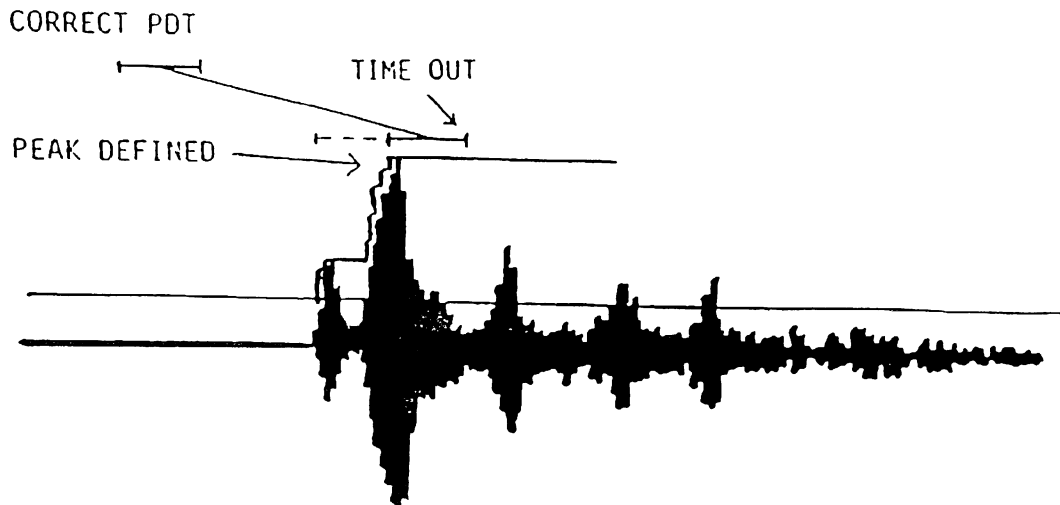


Figure A.2 Illustration of PDT Parameter

A.3 Hit Lockout Time

Hit lockout time is the amount of time that the system waits after the HDT, before it resets the system to read the next hit. The definition of HLT is shown graphically in Figure A.3. A typical value of HLT is 300 microseconds for fiberglass/epoxy, and this was the value used in these tests.

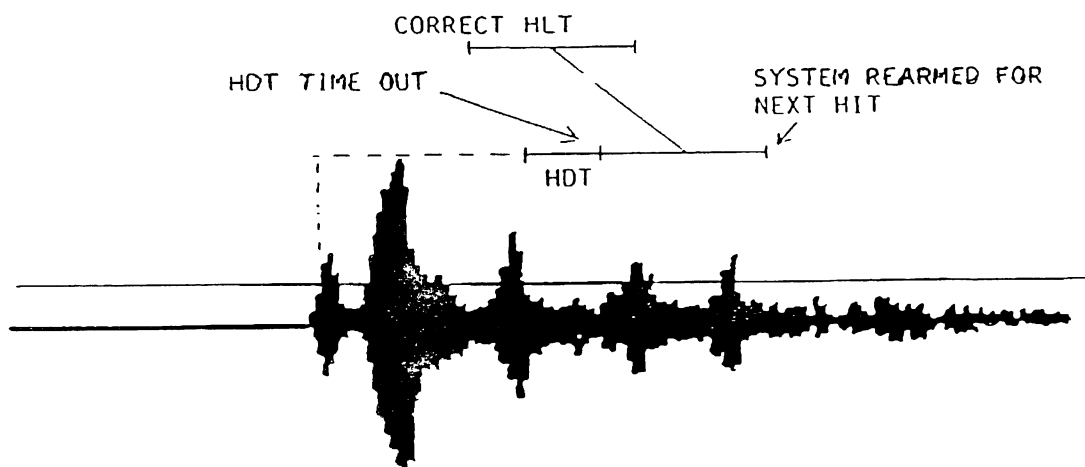


Figure A.3 Illustration of HLT Parameter

APPENDIX B
JOHNSON DISTRIBUTION CURVES

Mechanism 1

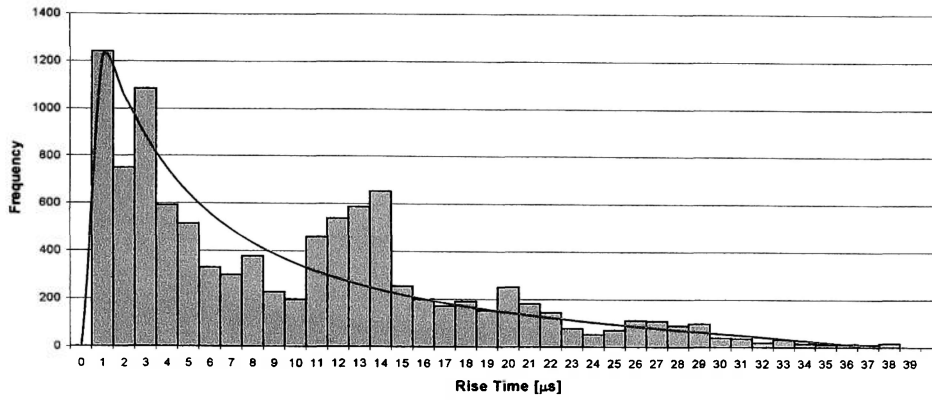


Figure B.1 Bounded Johnson Fit for the Rise Time Distribution, Mechanism 1

Mechanism 1

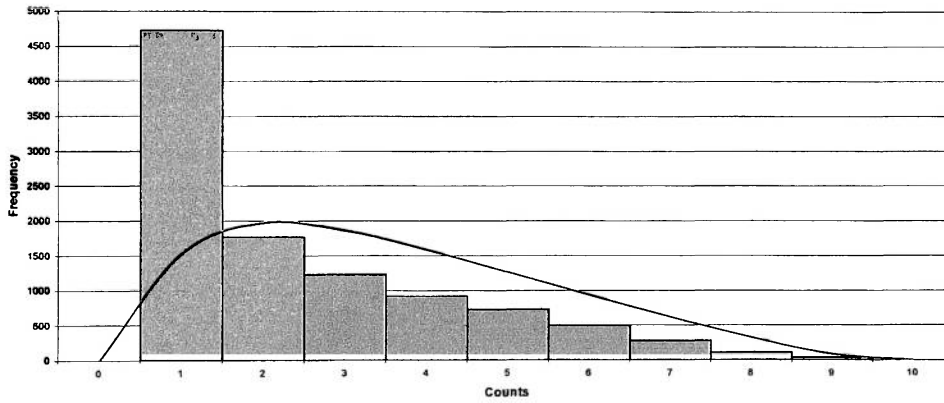


Figure B.2 Bounded Johnson Fit for the Counts Distribution, Mechanism 1

Mechanism 1

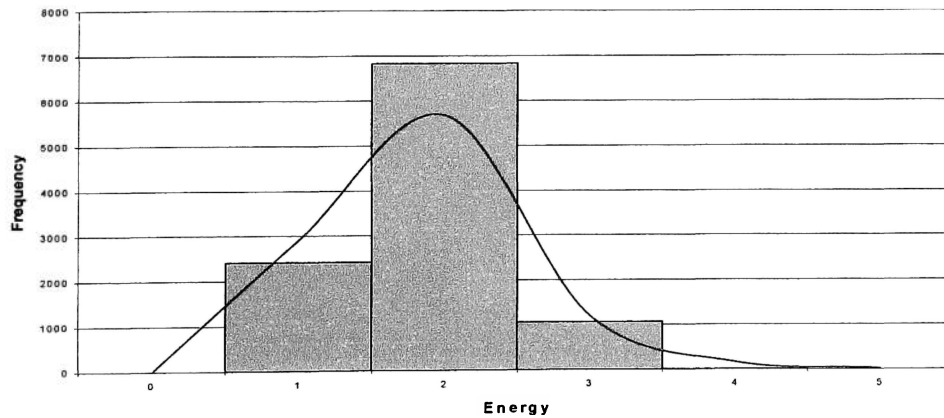


Figure B.3 Lognormal Johnson Fit for the Energy Distribution, Mechanism 1

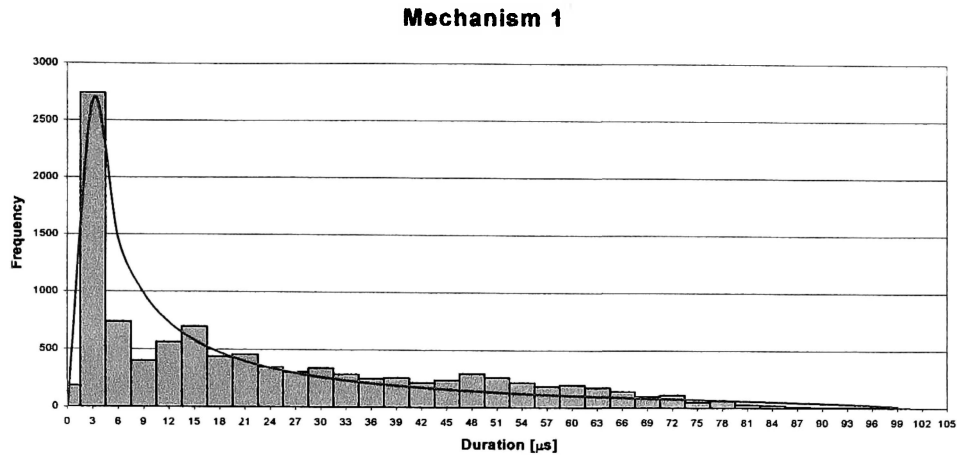


Figure B.4 Bounded Johnson Fit for the Duration Distribution, Mechanism 1

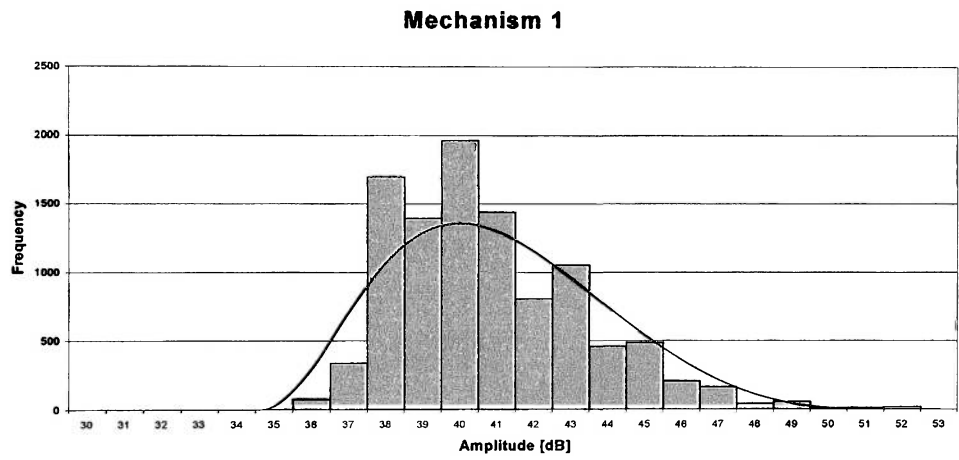


Figure B.5 Bounded Johnson Fit for the Amplitude Distribution, Mechanism 1

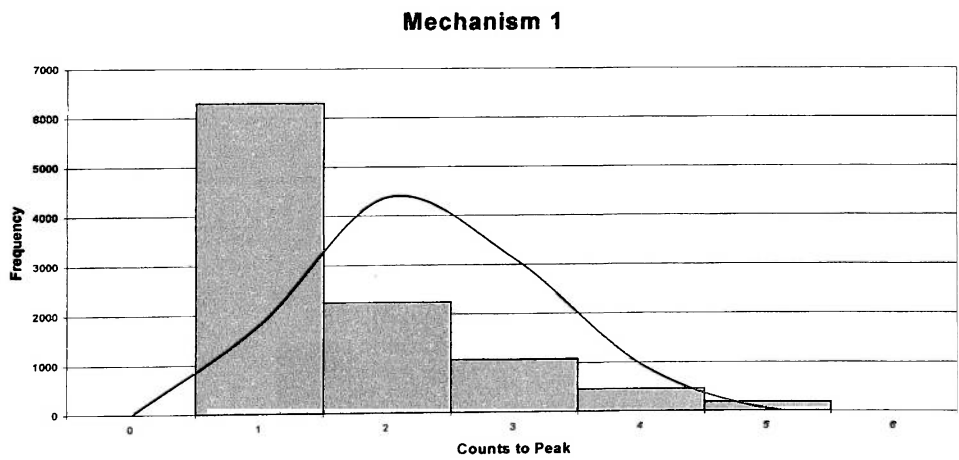


Figure B.6 Bounded Johnson Fit for the Counts to Peak Distribution, Mechanism 1

Mechanism 2

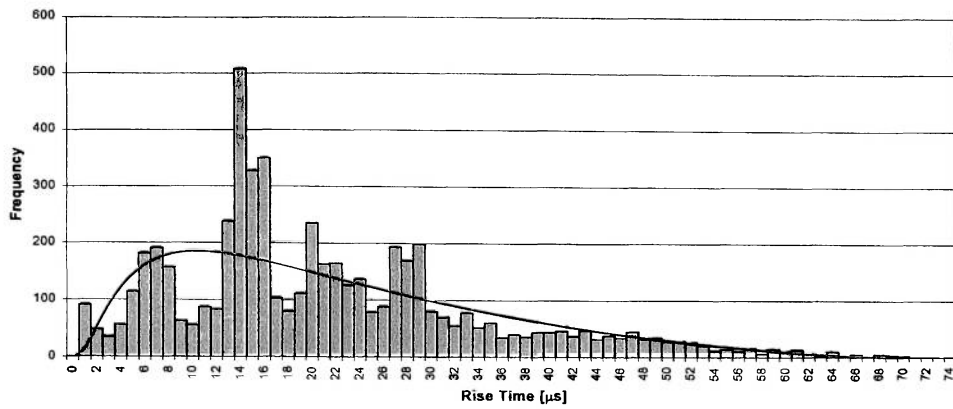


Figure B.7 Bounded Johnson Fit for the Rise Time Distribution, Mechanism 2

Mechanism 2

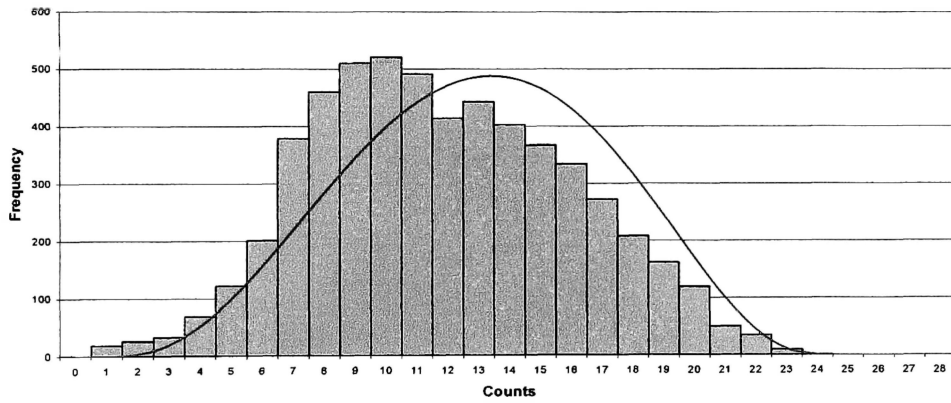


Figure B.8 Bounded Johnson Fit for the Counts Distribution, Mechanism 2

Mechanism 2

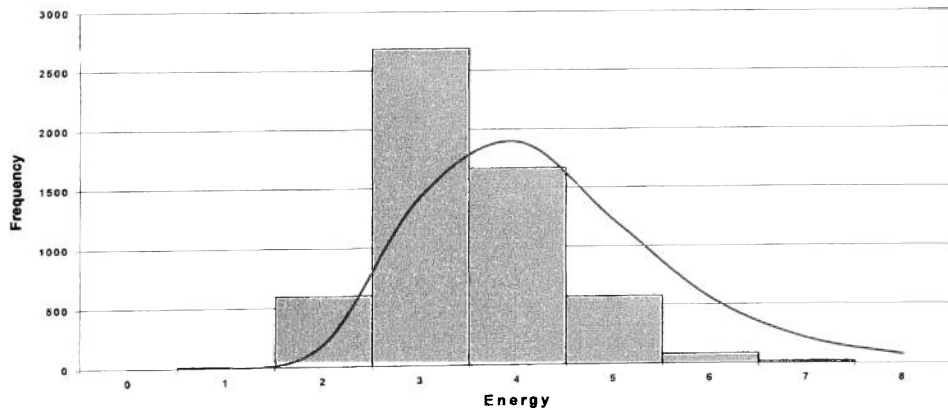


Figure B.9 Lognormal Johnson Fit for the Energy Distribution, Mechanism 2

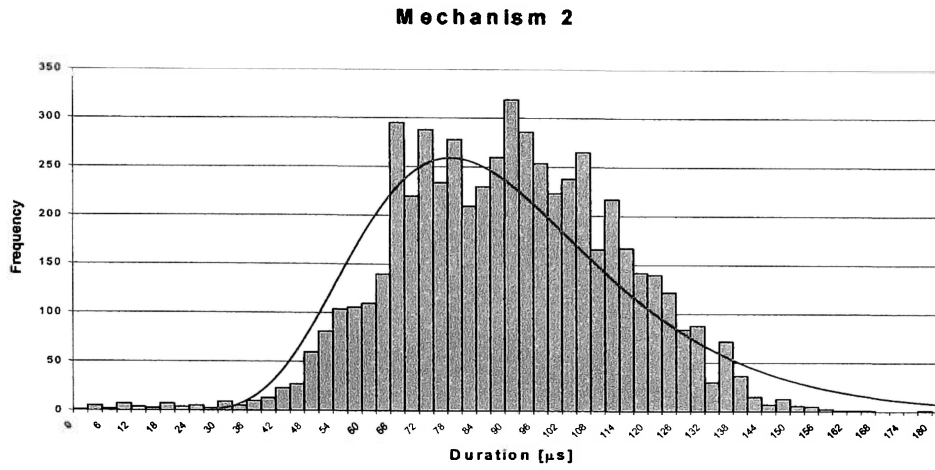


Figure B.10 Lognormal Johnson Fit for the Duration Distribution, Mechanism 2

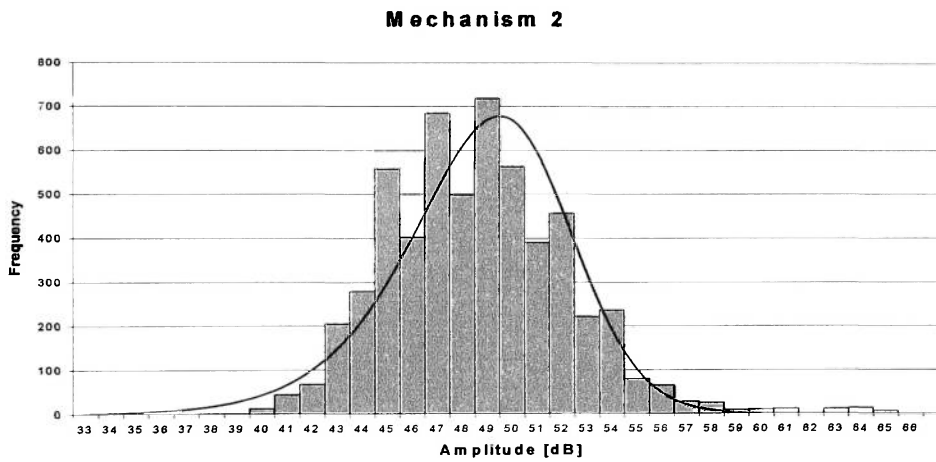


Figure B.11 Unbounded Johnson Fit for the Amplitude Distribution, Mechanism 2

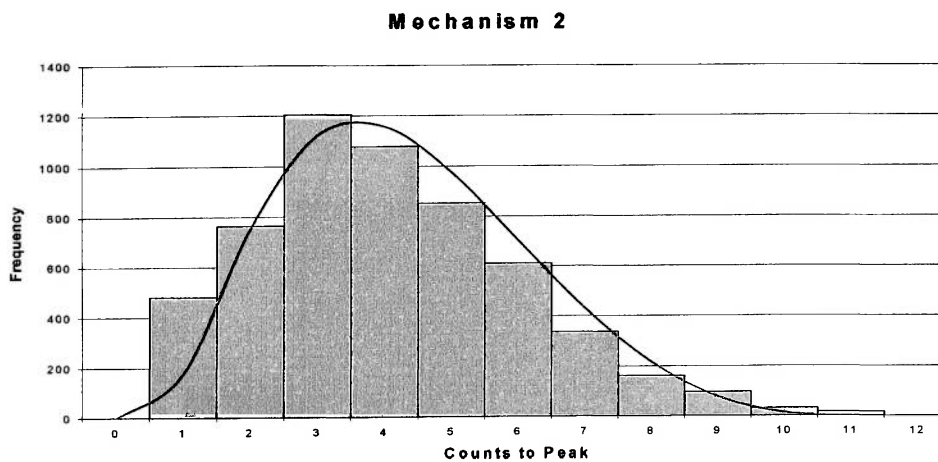


Figure B.12 Bounded Johnson Fit for the Counts to Peak Distribution, Mechanism 2

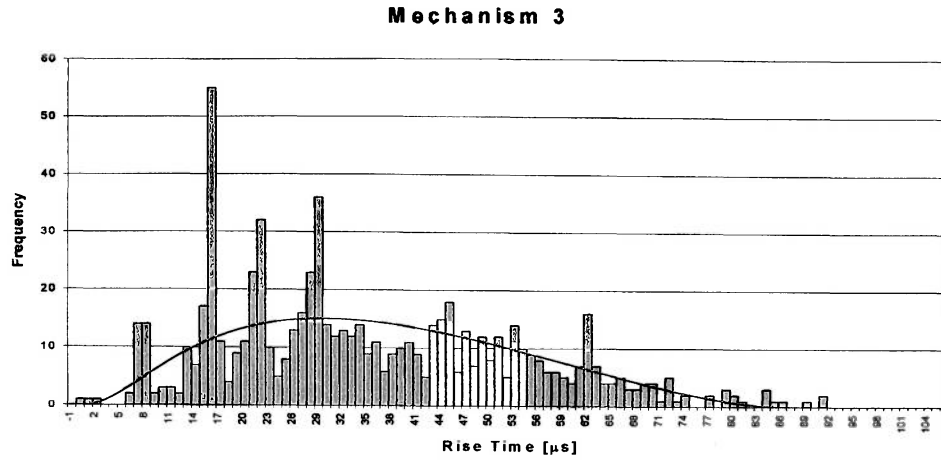


Figure B.13 Bounded Johnson Fit for the Rise Time Distribution, Mechanism 3

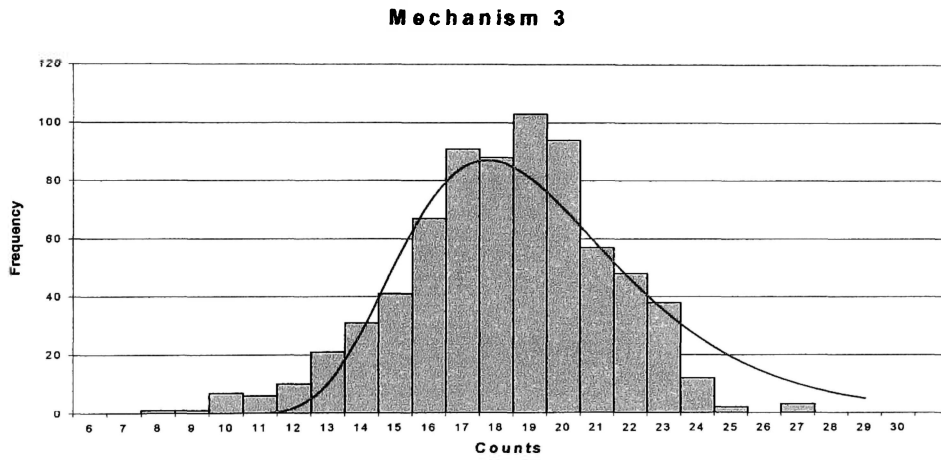


Figure B.14 Lognormal Johnson Fit for the Counts Distribution, Mechanism 3

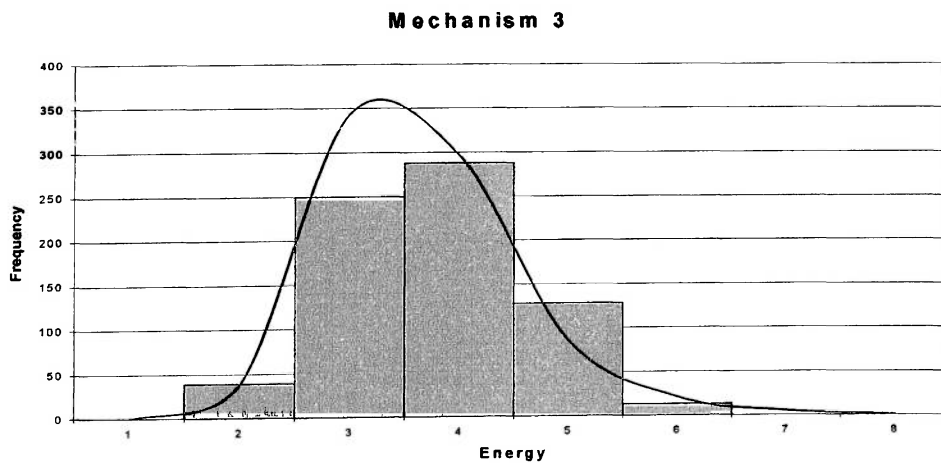


Figure B.15 Lognormal Johnson Fit for the Energy Distribution, Mechanism 3

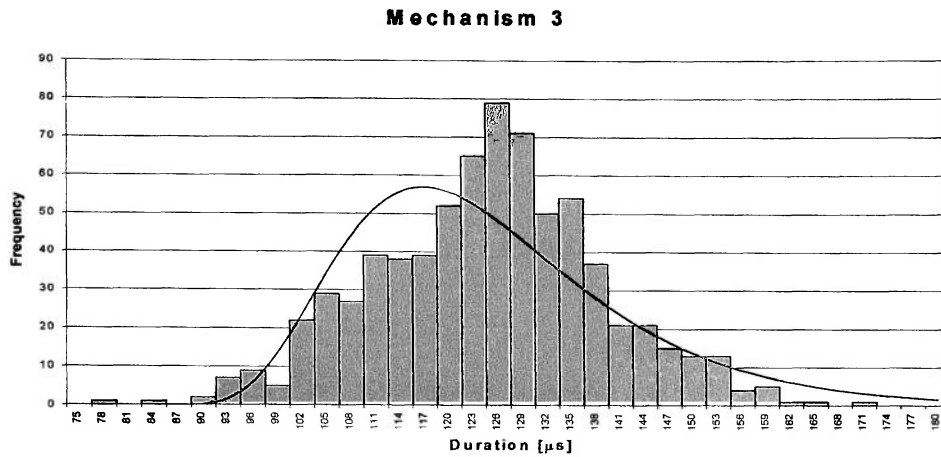


Figure B.16 Lognormal Johnson Fit for the Duration Distribution, Mechanism 3

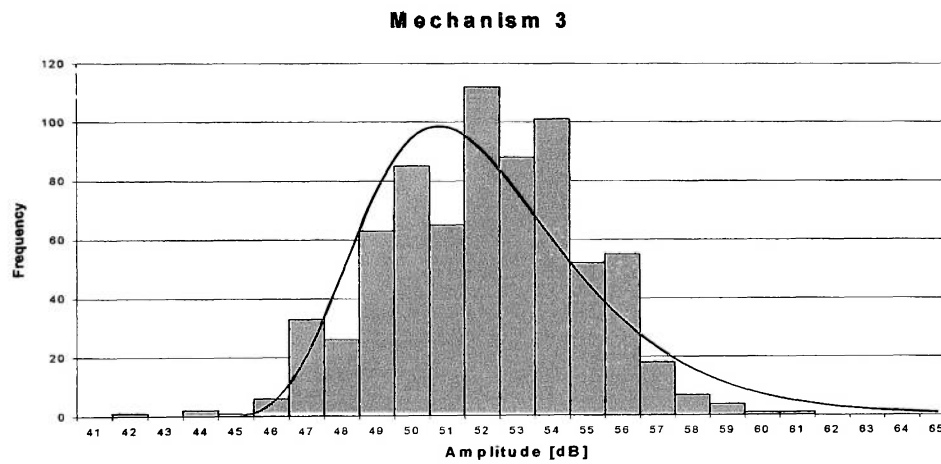


Figure B.17 Lognormal Johnson Fit for the Amplitude Distribution, Mechanism 3

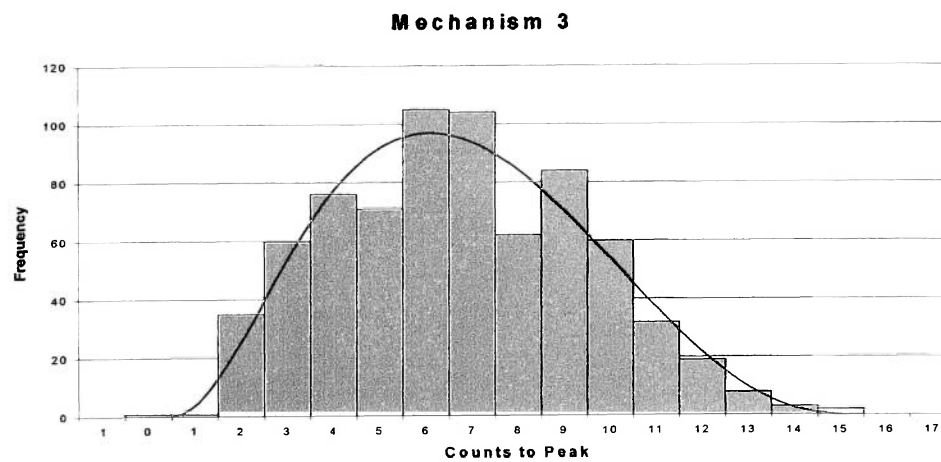


Figure B.18 Bounded Johnson Fit for the Counts to Peak Distribution, Mechanism 3

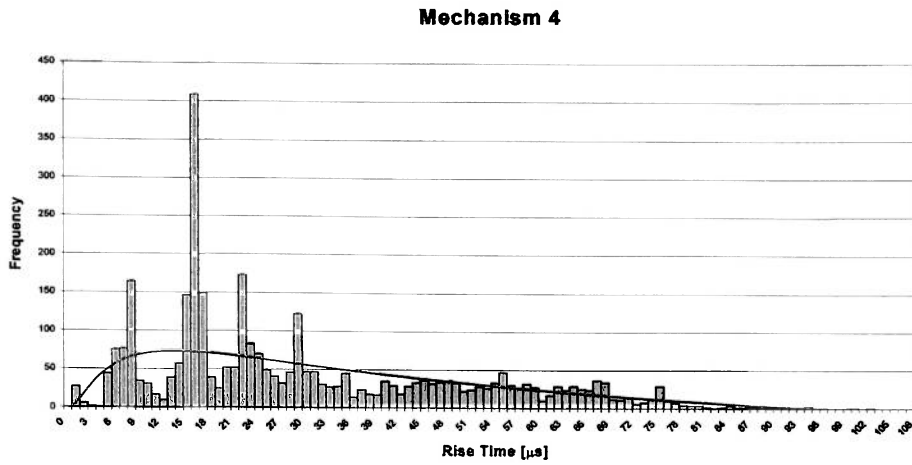


Figure B.19 Bounded Johnson Fit for the Rise Time Distribution, Mechanism 4

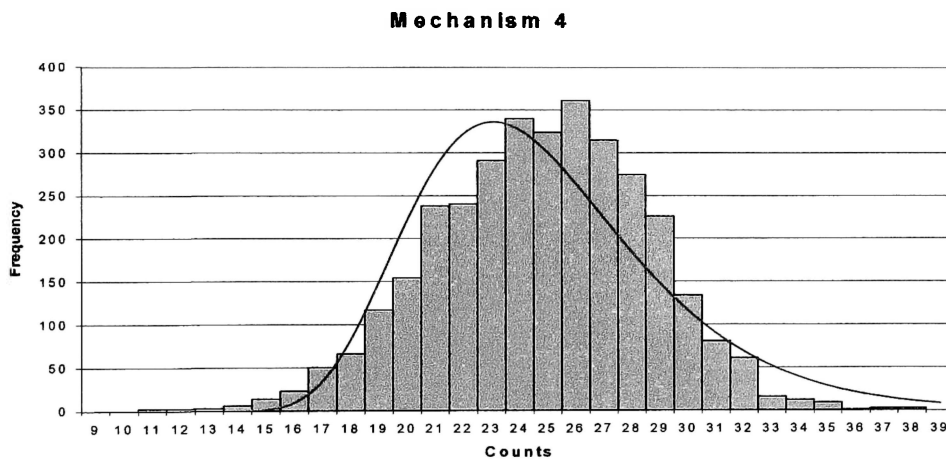


Figure B.20 Lognormal Johnson Fit for the Counts Distribution, Mechanism 4

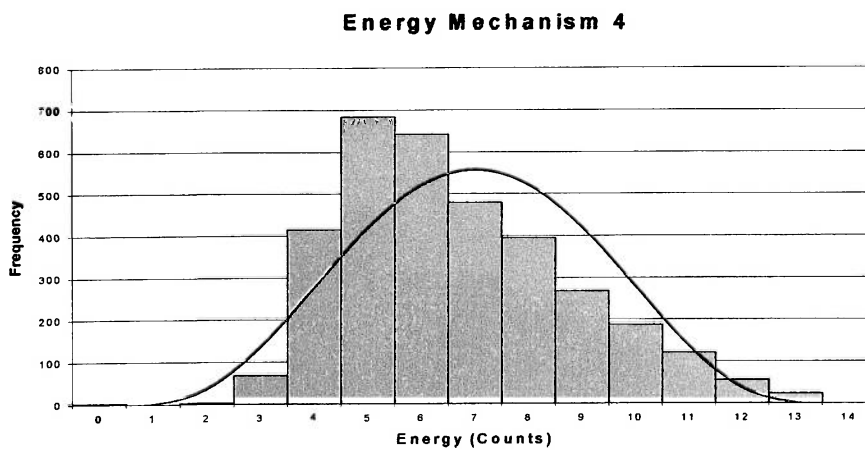


Figure B.21 Bounded Johnson Fit for the Energy Distribution, Mechanism 4

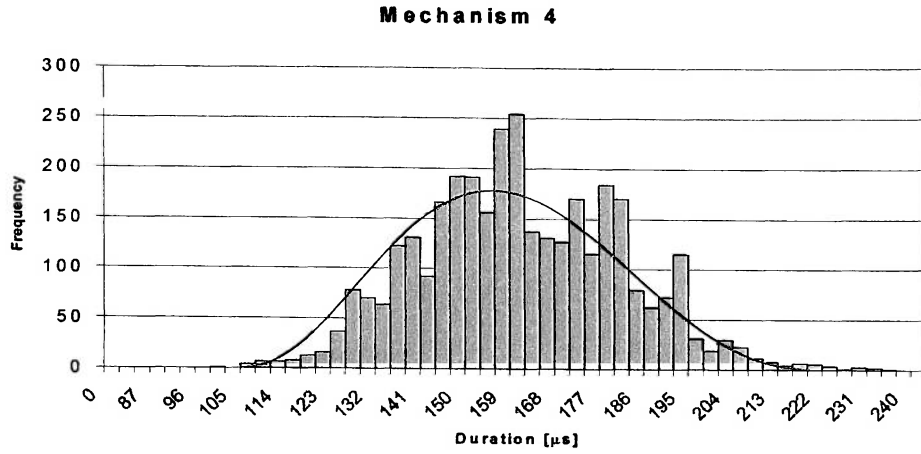


Figure B.22 Bounded Johnson Fit for the Duration Distribution, Mechanism 4

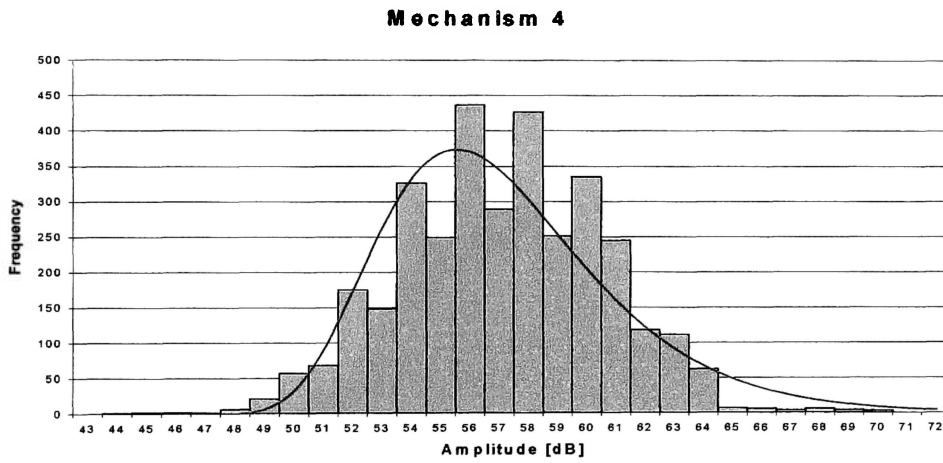


Figure B.23 Lognormal Johnson Fit for the Amplitude Distribution, Mechanism 4

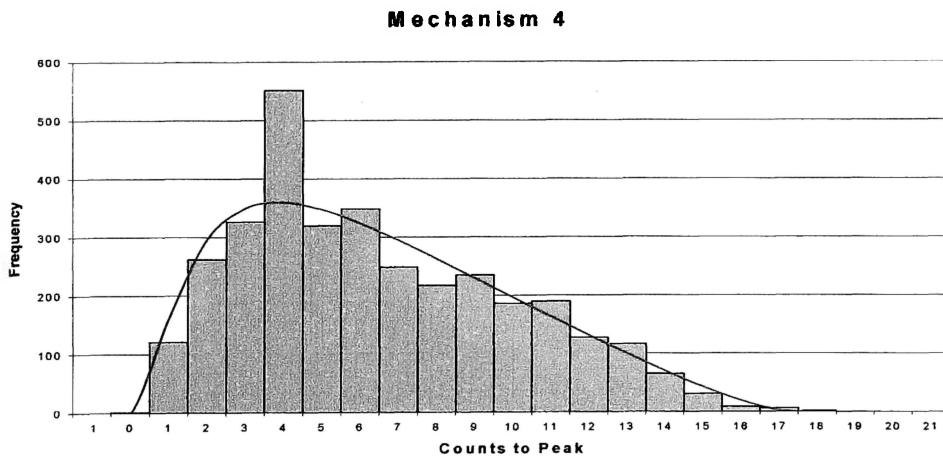


Figure B.24 Bounded Johnson Fit for the Counts to Peak Distribution, Mechanism 4

Mechanism 5

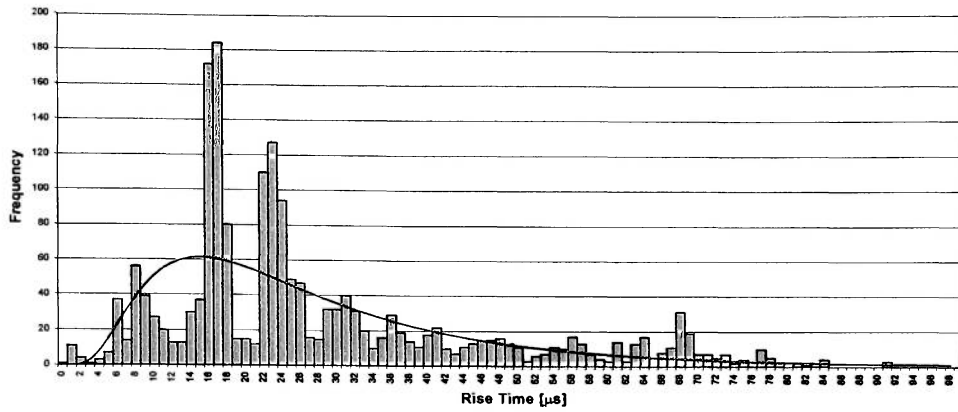


Figure B.25 Lognormal Johnson Fit for the Rise Time Distribution, Mechanism 5

Mechanism 5

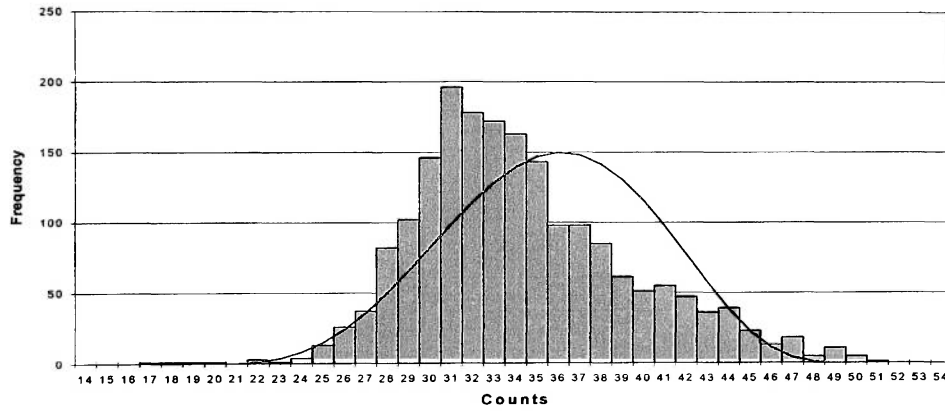


Figure B.26 Bounded Johnson Fit for the Counts Distribution, Mechanism 5

Mechanism 5

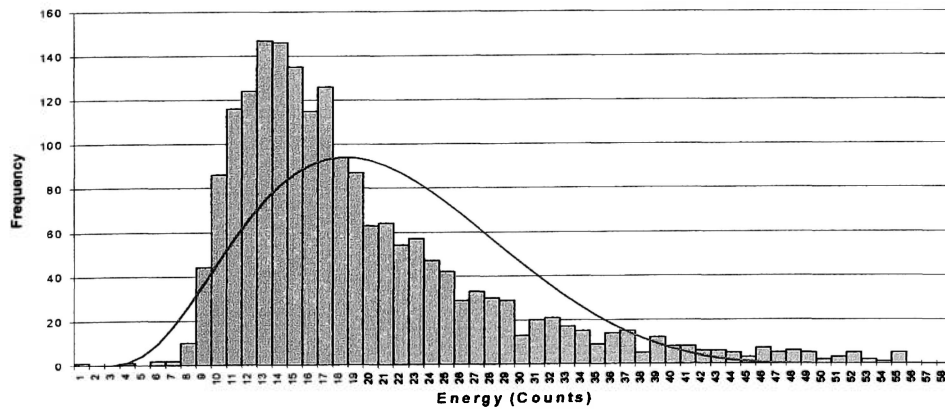


Figure B.27 Bounded Johnson Fit for the Energy Distribution, Mechanism 5

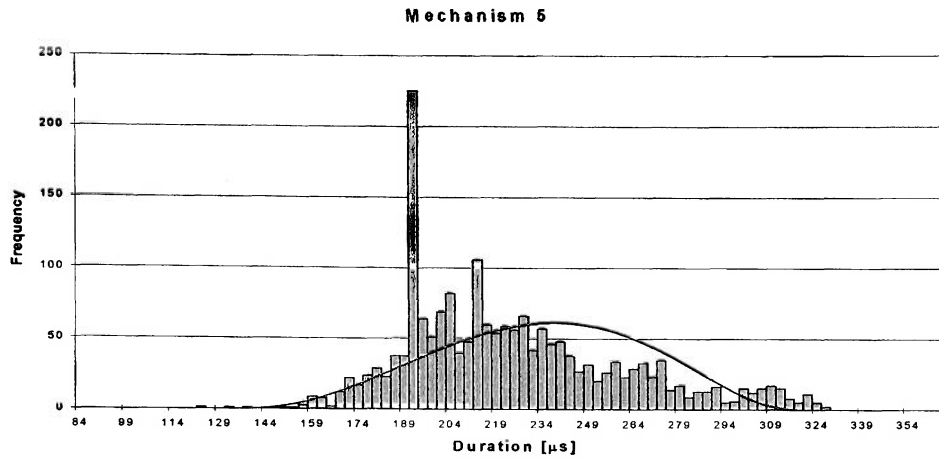


Figure B.28 Bounded Johnson Fit for the Duration Distribution, Mechanism 5

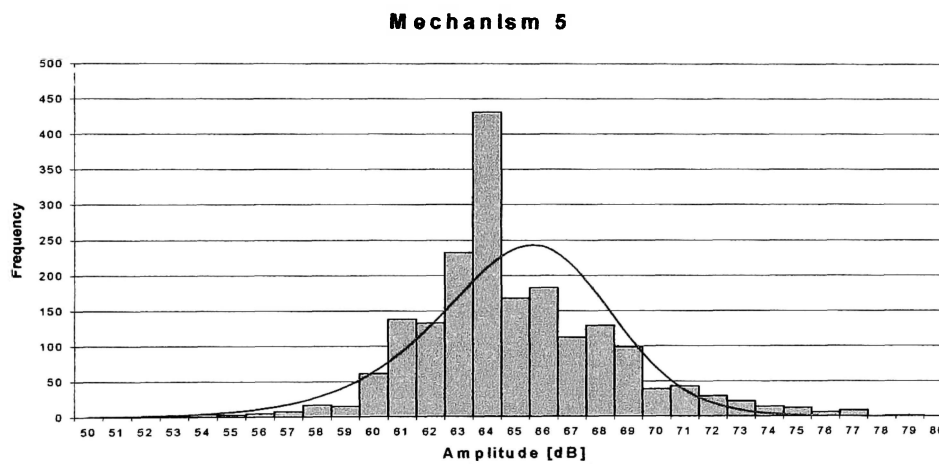


Figure B.29 Unbounded Johnson Fit for the Amplitude Distribution, Mechanism 5

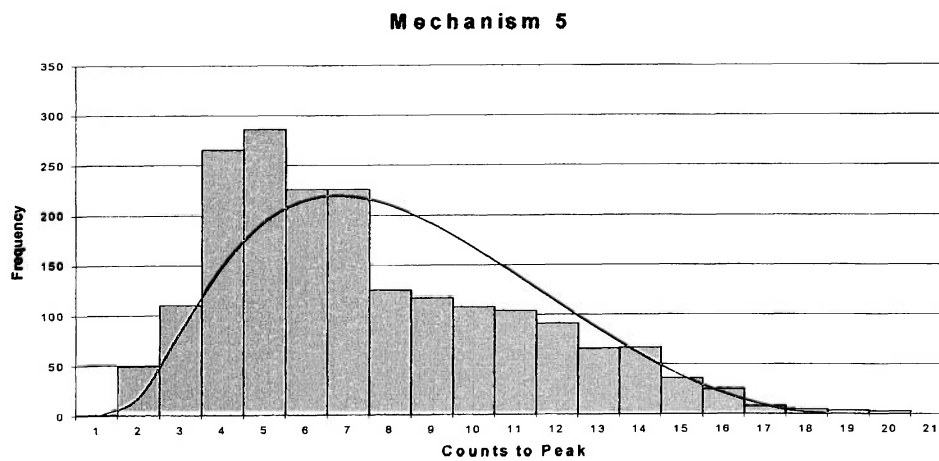


Figure B.30 Bounded Johnson Fit for the Counts to Peak Distribution, Mechanism